Improvement of DCT-based Compression Algorithms Using Poisson's Equation

Katsu Yamatani* and Naoki Saito, *Senior Member, IEEE*

Abstract

We propose two new image compression-decompression methods that reproduce images with better visual fidelity, less blocking artifacts, and better PSNR, particularly in low bit rates, than those processed by the JPEG Baseline method at the same bit rates. The additional computational cost is small, i.e., linearly proportional to the number of pixels in an input image. The first method, the "full mode" *polyharmonic local cosine transform* (PHLCT), modifies the encoder and decoder parts of the JPEG Baseline method. The second one, the "partial mode" PHLCT (or PPHLCT for short), only modifies the decoder part: it accepts the JPEG files, yet decompresses them with higher quality. The key idea behind these algorithms is a decomposition of each image block into a *polyharmonic* component and a *residual*. The polyharmonic component in this paper is an approximate solution to Poisson's equation with the Neumann boundary condition, which means that it is a smooth predictor of the original image block only using the image gradient information across the block boundary. Thus the residual—obtained by removing the polyharmonic component from the original image block—has approximately zero gradient across the block boundary, which gives rise to the fast-decaying DCT coefficients, which in turn lead to more efficient compression-decompression algorithms for the same bit rates. We show that the polyharmonic component of each block can be estimated solely by the first column and row of the DCT coefficient matrix of that block and those of its adjacent blocks and can predict an original image data better than some of the other AC prediction methods previously proposed. Our numerical experiments objectively and subjectively demonstrate the superiority of PHLCT over the JPEG Baseline method and the improvement of the JPEG-compressed images when decompressed by PPHLCT.

EDICS Category: 1-STIL, 1-STAN, 2-NFLT, 2-REST

K. Yamatani is with the Department of Systems Engineering, Shizuoka University, 3-5-1 Johoku, Hamamatsu, Shizuoka 432-8561 Japan (e-mail: yamatani@sys.eng.shizuoka.ac.jp, tel/fax:+81-53-478-1220).

N. Saito is with the Department of Mathematics, University of California, Davis, One Shield Avenue, Davis, CA 95616-8633 USA (e-mail: saito@math.ucdavis.edu, tel:530-754-2121 fax:530-752-6635).

Advanced Coding Exhibit No. 2005, IPR2024-00374
Page 001

I. Introduction

Currently, the most popular image compression scheme is the JPEG standard for still images and the MPEG standard for video sequences. Although new standards such as JPEG-2000 and MPEG-21 (both of them have adopted wavelets) are emerging, many systems including digital cameras and image databases still use the JPEG standard [1], [2], which is based on the *Discrete Cosine Transform* (DCT) [3], [4], [5]. The reasons why DCT—sometimes called DCT Type II or DCT-II [4], [5]—is used in many compression algorithms instead of the Discrete Fourier Transform (DFT) or the Discrete Sine Transform (DST) are the following.

1) DCT theoretically approximates the Karhunen-Loève Transform (KLT) if we assume the first order Markov property in a given set of signals to be compressed [6]. It is well known that KLT is the most efficient *linear* transform for a collection of signals if the reconstruction error is measured in the mean square error (MSE) [6], [7].
2) Even more important is its treatment of the block boundaries. Taking DCT of an image block is equivalent to: a) extending the data by even reflection at the block boundaries; b) taking DFT of the extended data by viewing it as periodic with the period twice as long as that of the original block; and c) discarding $3/4$ of the resulting coefficients that were created by the even reflection and extension. This implies that DCT views the data as a *continuous* function across the block boundaries as long as there is no intrinsic singularity within the block. This should be contrasted with DFT and DST: they view the data as *discontinuous* across the block boundaries *even if there is no intrinsic singularity within the block*. This leads to the faster decay of the DCT coefficients than the DFT or DST coefficients, which is a desirable property in any transform coding system because it allows us to approximate the original data with a fewer number of terms in the series expansion used in the transform. More precisely, let $F_{\boldsymbol{k}}$ be the $\boldsymbol{k}$th DCT coefficient of an image block, where $\boldsymbol{k} = (k_1, k_2)$ is a pair of indices specifying the spatial frequencies along vertical and horizontal directions. Then, one can show that $|F_{\boldsymbol{k}}| \leq C\|\boldsymbol{k}\|^{-2} = C/(k_1^2 + k_2^2)$ for some constant $C > 0$ (see also Section II). We denote this by $F_{\boldsymbol{k}} = O(\|\boldsymbol{k}\|^{-2})$ in this paper. On the other hand, the magnitude of the DFT and DST coefficients of the same block is of $O(\|\boldsymbol{k}\|^{-1})$, i.e., those decay slower than the DCT coefficients. See Theorem 1 in Section II for the precise statement relating the smoothness of a function and the decay rate of its Fourier coefficients.
3) The lowest frequency basis vector of DCT is completely flat, i.e., truly measuring the important "DC" component of an image block, which is not the case in DST and in the other versions of

Advanced Coding Exhibit No. 2005, IPR2024-00374
Page 002

DCT called DCT Type I, III, and IV (see e.g., [4], [5]).

Although DCT-based codecs, such as the JPEG Baseline sequential codec, are quite popular, there are two problems in them that we want to overcome. First, the decay rate $O(\|\boldsymbol{k}\|^{-2})$ of the DCT coefficients is still too slow. We would like to make the transformed coefficients decay faster in order to achieve better compression. Second, such codecs generate the infamous blocking artifacts (visible discontinuities between adjacent blocks) when the compressed data—especially the ones with low bit rates—are decompressed, which are quite noticeable and annoying for human observers. Many techniques have been developed to remove the blocking artifacts while keeping the objectively measured image quality (e.g., PSNR) constant, e.g., [8], [9], [10], [11], [12]. These all operate on the spatial domain, i.e., these are post-processing techniques after the decompression is done. On the other hand, another set of techniques has been suggested as an option in the JPEG standard [1, Sec. 16.1] and further explored in [14], [15], [18]. These methods are all based on the prediction of the AC coefficients by fitting quadratic or cubic polynomial surface using the DC coefficients of several blocks. In general, polynomial surface fitting techniques are effective to remove the blocking artifacts especially for images compressed in low bit rates. However, for the actual implementation of these techniques, there is a common difficulty to distinguish intrinsic singularities in the original image from the artificial discontinuities that cause the blocking artifacts.

To address these problems, Saito and Remy recently developed a new transform called *Polyharmonic Local Sine Transform* (PHLST) [19], [20]. PHLST gives rise to the transform coefficients decaying as $O(\|\boldsymbol{k}\|^{-3})$ or faster as we shall review in Section II-C. Although PHLST is very promising in certain applications such as local feature computation, directional derivatives estimation, image interpolation, and image zooming, it cannot directly and fully utilize the infrastructure of the JPEG Baseline method due to its use of DST instead of DCT as well as its storage requirement of the block boundary information.

In this paper, we propose the *Polyharmonic Local Cosine Transform* (PHLCT) that compensates these problems of PHLST: it gives us the coefficients decaying as $O(\|\boldsymbol{k}\|^{-4})$, yet fully utilizes the JPEG Baseline infrastructure. There are two modes in PHLCT. One is the *full* mode that modifies the encoder and decoder parts of the JPEG Baseline procedure. The other is what we call the *partial* mode. This mode modifies only the decoder part. Our methods can also be viewed as new and improved AC prediction methods over the previously proposed ones, e.g., [1, Sec. 16.1], [14], [15], [17], and [18].

The organization of this paper is as follows. In Section II, we set our notation and review the Fourier cosine series and PHLST. In Section III, we propose PHLCT and show why the Fourier cosine coefficients of the residual decay as $O(\|\boldsymbol{k}\|^{-4})$. Section IV describes how to compute the PHLCT representation

Advanced Coding Exhibit No. 2005, IPR2024-00374
Page 003

of an input image from the DCT coefficients of that image. In Section V, we derive more practical approximation of the polyharmonic component than that in Section IV solely using the DC components of the current and adjacent blocks. Then we describe our compression-decompression algorithms using full and partial modes of PHLCT in Section VI. Section VII describes our numerical experiments. There we compare the performance of our methods in predicting the original AC coefficients with that of the other AC prediction methods mentioned above. Also, we quantify the image quality improvement of our methods over the JPEG Baseline method using several image quality measures. We finally conclude our paper in Section VIII with our future plan.

II. Review of Fourier Cosine Series Expansion and Polyharmonic Local Sine Transform

In this section and the next, we shall deal with data in an arbitrary dimension $n \in \mathbb{N}$ since our method may be useful for compressing not only 2D images but also 3D data such as 3D seismic data. We shall then focus on the case of $n = 2$ for images starting Section IV.

A. Fourier series expansion and periodization

Let Ω be a block domain $\Omega = \{\boldsymbol{x} \in \mathbb{R}^n | 0 < x_i < 1, i = 1, 2, \ldots, n\}$, where $\boldsymbol{x} = (x_1, x_2, \ldots, x_n)$. Let us now consider a function f defined on the closed domain $\overline{\Omega} = \Omega \cup \partial\Omega$, where $\partial\Omega$ denotes the boundary of Ω. Then let us extend it periodically over the whole space $\mathbb{R}^n$, and let $\widetilde{f}$ be this periodic extension of f. We have the following basic theorem that relates the decay rate of the Fourier coefficients and the smoothness of the function $\widetilde{f}$. For the details and the proof, see Appendix in [20].

Theorem 1: Let f be a function defined on $\overline{\Omega} \in \mathbb{R}^n$ and $\widetilde{f}$ be its periodic extension to $\mathbb{R}^n$. Furthermore, let us assume that 1) $\widetilde{f} \in C^m(\mathbb{R}^n)$, where m is some nonnegative integer; and 2) $\partial^{m+1}\widetilde{f}/\partial x_j^{m+1}$, $j = 1, \ldots, n$, exists and of bounded variation in Ω. Then the Fourier coefficient $c_{\boldsymbol{k}}$ of f decays as $O(\|\boldsymbol{k}\|^{-m-2})$, $\boldsymbol{k} = (k_1, \ldots, k_n) \in \mathbb{Z}^n$, and $\|\boldsymbol{k}\|$ is the Euclidean (i.e., ℓ^2) norm of $\boldsymbol{k}$.

Note that if some head and tail of f do not match, i.e., unless we have $f(x_1, \ldots, x_{i-1}, 0, x_{i+1}, \ldots, x_n) = f(x_1, \ldots, x_{i-1}, 1, x_{i+1}, \ldots, x_n)$ for all $i \in \{1, \ldots, n\}$ and all x_k with $0 \le x_k \le 1$, $k \neq i$, which is almost always violated in real data, then the periodic extension $\widetilde{f}$ becomes discontinuous. Thus its Fourier coefficients decay only as $O(\|\boldsymbol{k}\|^{-1})$ and reveal the infamous Gibbs phenomenon.

B. Fourier cosine series expansion and even reflection

We now consider the Fourier cosine series expansion of such a nonperiodic function $f \in C^{m'}(\overline{\Omega})$ for some $m' \in \mathbb{N}$. Because of the equivalence of the Fourier cosine series expansion of f and the complex

Advanced Coding Exhibit No. 2005, IPR2024-00374
Page 004

Fourier series expansion of the even-reflected version of f as briefly discussed in Introduction, the even-reflected version becomes at least continuous and periodic over the extended domain $[-1,1]^n$. Thus, applying Theorem 1 with $m=0$, the Fourier cosine coefficients of f decay as $O(\|\boldsymbol{k}\|^{-2})$. Unfortunately, even if f is sufficiently smooth on the block, i.e., $f \in C^{m'}(\overline{\Omega})$ with large positive m' including the case of $m' = \infty$, there is no guarantee that the even reflection preserves the continuity of the derivatives across the boundary. Therefore, the Fourier cosine coefficients cannot decay faster than $O(\|\boldsymbol{k}\|^{-2})$ in general.

C. Polyharmonic local sine transform

In order to have expansion coefficients decaying as $O(\|\boldsymbol{k}\|^{-3})$ or faster without generating Gibbs oscillations, Saito and Remy proposed the *Polyharmonic Local Sine Transform* (PHLST) [19], [20]. PHLST also compensates several problems in the local trigonometric transforms (LTTs) of Coifman and Meyer [21] and Malvar [22], [23], such as the overlapping windows and the slope of the bell functions. PHLST first segments a given function f supported on Ω by splitting it into a set of disjoint blocks $\{\Omega_j\}_{j=1}^J$ for some $J \in \mathbb{N}$ such that $\overline{\Omega} = \cup_{j=1}^J \overline{\Omega}_j$ using the characteristic functions. Let f_j be the restriction of f to $\overline{\Omega}_j$, i.e., $f_j = \chi_{\overline{\Omega}_j} f$. Then PHLST decomposes each f_j into two components as $f_j = u_j + v_j$. The components u_j and v_j are referred to as the *polyharmonic component* and the *residual*, respectively. The polyharmonic component is obtained by solving the following *polyharmonic equation*:

$$\Delta^m u_j = 0 \quad \text{in } \Omega_j, \quad m = 1, 2, \ldots \tag{1}$$

with given boundary values and normal derivatives

$$\frac{\partial^{q_\ell} u_j}{\partial \nu^{q_\ell}} = \frac{\partial^{q_\ell} f}{\partial \nu^{q_\ell}} \quad \text{on } \partial\Omega_j, \quad \ell = 0, \ldots, m-1, \tag{2}$$

where $\Delta = \sum_{i=1}^n \partial^2/\partial x_i^2$ is the Laplace operator in $\mathbb{R}^n$, the natural number m is called a degree of polyharmonicity, and q_ℓ is the order of the normal derivatives that needs to be specified. The first order normal derivative $\partial f/\partial \nu$ at $\boldsymbol{x} \in \partial\Omega_j$ is defined as $\boldsymbol{\nu}(\boldsymbol{x}) \cdot \nabla f(\boldsymbol{x})$, where $\boldsymbol{\nu}(\boldsymbol{x})$ is a normal vector perpendicular to the boundary $\partial\Omega_j$ at $\boldsymbol{x}$ pointing to the outside of Ω_j. The higher order normal derivatives can be defined recursively. The parameter q_0 is normally set to 0, which means that $u_j = f$ on the boundary $\partial\Omega_j$, which is called the Dirichlet boundary condition. These boundary conditions (2) enforce the function values and the normal derivatives of orders $q_1, \ldots, q_{m-1}$ of the solution u_j along the boundary $\partial\Omega_j$ to match those of the original signal f over there. If the Ω_j's are all rectangles (of possibly different sizes), then PHLST sets $q_\ell = 2\ell$ in (2), i.e., it constrains the *even order* normal derivatives. It is not necessary to match the odd order normal derivatives for the rectangular domain case because the Fourier

Advanced Coding Exhibit No. 2005, IPR2024-00374
Page 005

sine series of v_j is equivalent to the complex Fourier series expansion of the extension of v_j by odd reflection with respect to the boundary $\partial\Omega_j$ and *the continuity of the odd order normal derivatives (up to order $2m-1$) is automatically guaranteed*. Note that for $m = 1, 2$, Eq. (1) is usually called Laplace's equation and the biharmonic equation, respectively. Note also that in 1D ($n = 1$), u_j for $m = 1$ is simply a straight line connecting two boundary points of an interval $\overline{\Omega}_j$ whereas in the $m = 2$ case, it is a cubic polynomial. However, note that in higher dimensions ($n \geq 2$), the solution of (1) with (2) is not a tensor product of algebraic polynomials in general. Subtracting such u_j from f_j gives us the residual $v_j = f_j - u_j$ satisfying

$$\frac{\partial^{q_\ell} v_j}{\partial \nu^{q_\ell}} = 0 \quad \text{on } \partial\Omega_j, \quad \ell = 0, \ldots, m-1.$$

Since the values and the normal derivatives of v_j on $\partial\Omega_j$ vanish, its Fourier sine expansion coefficients decay rapidly, i.e., $O(\|\boldsymbol{k}\|^{-2m-1})$, if there is no other intrinsic singularity in Ω_j. In fact, we have the following theorem.

Theorem 2: Let Ω_j be a bounded rectangular domain in $\mathbb{R}^n$, and let $f_j \in C^{2m}(\overline{\Omega}_j)$, but non-periodic. Assume further that $(\partial/\partial x_i)^{2m+1} f$, $i = 1, \ldots, n$, exist and are of bounded variation. Furthermore, let $f_j = u_j + v_j$ be the PHLST representation, i.e., the polyharmonic component u_j is the solution of the polyharmonic equation (1) of degree m and the boundary condition (2) with $q_\ell = 2\ell$, $\ell = 0, 1, \ldots, m-1$, and $v_j = f_j - u_j$ is the residual. Then, the Fourier sine coefficient $b_{\boldsymbol{k}}$ of the residual v_j is of $O\left(\|\boldsymbol{k}\|^{-2m-1}\right)$ for all $\boldsymbol{k} \neq \boldsymbol{0}$, where $\boldsymbol{k} = (k_1, \ldots, k_n) \in \mathbb{Z}_+^n$.

The proof of this theorem can be found in [20]. We call this way of decomposing a function f into a set of functions $\{f_j = u_j + v_j\}_{j=1}^J$ the *Polyharmonic Local Sine Transform* (PHLST) with degree of polyharmonicity m. The polyharmonic components can be computed quickly by utilizing the computationally-fast and numerically-accurate Laplace/Poisson solver developed by Averbuch, Braverman, Israeli, and Vozovoi [24], [25] as long as the boundary data are stored and the normal derivatives at the boundary are available. Combining this feature with the quickly decaying expansion coefficients of the residuals, the usefulness of PHLST with $m = 1$ to image approximation was demonstrated [19], [20]. In this case, the Fourier sine coefficients of the v_j component decay as $O(\|\boldsymbol{k}\|^{-3})$ if $f_j \in C^2(\overline{\Omega}_j)$. However, for $m \geq 2$, we need to estimate the normal derivatives at the block boundary using the sampled data, and consequently, it becomes more difficult to deal with in practice. See [26] for more about the estimation of normal derivatives and related issues. Also, PHLST cannot utilize the infrastructure of the JPEG standard since it is based on DST instead of DCT.

Advanced Coding Exhibit No. 2005, IPR2024-00374
Page 006

III. Polyharmonic Local Cosine Transform

The disadvantages of PHLST described in the previous section motivated us to develop a cosine version of the transform, the *polyharmonic local cosine transform* (PHLCT). Our goal is to find a decomposition $f_j = u_j + v_j$ so that: 1) it is based on the Fourier cosine series expanion of the v_j components for the compatibility with the JPEG standard; and 2) the expansion coefficients decay as $O(\|\boldsymbol{k}\|^{-4})$ or faster.

Our strategy for achieving these is the following. We modify the boundary condition (2) by setting $q_\ell = 2\ell+1$, $\ell = 0, \ldots, m-1$. If we use this set of boundary conditions, then in priciple, it is possible to obtain the v_j component whose Fourier cosine coefficients decay as $O(\|\boldsymbol{k}\|^{-2m-2})$. To proceed further, however, let us focus on the case of $m = 1$ due to the impracticality of estimating the normal derivatives of order higher than 1 as we mentioned previously. For $m = 1$, the u_j component should satisfy Laplace's equation with the so-called *Neumann boundary condition*:

$$\begin{cases} \Delta u_j = 0 & \text{in } \Omega_j, \\ \dfrac{\partial u_j}{\partial \nu} = \dfrac{\partial f}{\partial \nu} & \text{on } \partial\Omega_j. \end{cases} \tag{3}$$

However, this equation cannot have a solution in general, and we need to introduce the source term in the righthand side of Laplace's equation [27, Sec. 2D]. The reason is due to Green's second identity, which claims that for any $u, v \in C^1(\overline{\Omega}_j)$,

$$\int_{\Omega_j} (u\Delta v - v\Delta u)\, \mathrm{d}\boldsymbol{x} = \int_{\partial\Omega_j} \left(u\frac{\partial v}{\partial \nu} - v\frac{\partial u}{\partial \nu} \right) \mathrm{d}\sigma(\boldsymbol{x}), \tag{4}$$

where $\mathrm{d}\sigma(\boldsymbol{x})$ is a surface (or boundary) measure. Setting $u = u_j$ and $v = 1$ in (4) together with the Neumann boundary condition in (3), we have

$$\int_{\Omega_j} \Delta u_j \, \mathrm{d}\boldsymbol{x} = \int_{\partial\Omega_j} \frac{\partial u_j}{\partial \nu} \, \mathrm{d}\sigma(\boldsymbol{x}) = \int_{\partial\Omega_j} \frac{\partial f}{\partial \nu} \, \mathrm{d}\sigma(\boldsymbol{x}). \tag{5}$$

This is a necessary condition that u_j must satisfy. Therefore, we need to introduce the constant source term in Laplace's equation (3) as

$$\begin{cases} \Delta u_j = K_j & \text{in } \Omega_j, \\ \dfrac{\partial u_j}{\partial \nu} = \dfrac{\partial f}{\partial \nu} & \text{on } \partial\Omega_j, \end{cases} \tag{6}$$

where $K_j := \frac{1}{|\Omega_j|} \int_{\partial\Omega_j} \partial f / \partial \nu \, \mathrm{d}\sigma(\boldsymbol{x})$, $|\Omega_j|$ is the volume of the block Ω_j. It is easy to see that with this constant source term, the solution of (6) satisfies (5). Laplace's equation with the source term is called *Poisson's equation* [27, Chap. 2]. It is a well-known fact that (6) has a unique solution modulo an additive constant; see e.g., [27, Sec. 2D].

Advanced Coding Exhibit No. 2005, IPR2024-00374
Page 007

The solution u_j to (6) is not just a function having the matching normal derivative at the boundary with the original function f; the following theorem further characterizes u_j:

Theorem 3: Let p be a $C^2(\overline{\Omega}_j)$ function and $M(p)$ be the total squared curvature integral defined by

$$M(p) := \int_{\Omega_j} (\Delta p)^2 \, \mathrm{d}\boldsymbol{x} \, .$$

For any p with $\partial p/\partial \nu = \partial f/\partial \nu$ on $\partial\Omega_j$, the solution u_j to (6) satisfies $M(u_j) \leq M(p)$. In other words, the solution u_j is the minimizer of the total squared curvature integral on Ω_j.

The proof of this theorem can be found in Appendix. Theorem 3 guarantees that the influence of the boundary data to the entire shape of u_j is kept to a minimum in terms of the mean curvature. The u_j component can also be viewed as a smooth predictor of the original block f_j solely based on the gradient information across the block boundary.

Once we get the solution u_j, the residual $v_j = f_j - u_j$ clearly satisfies $\partial v_j/\partial \nu = 0 \quad$ on $\partial\Omega_j$. Since $f_j \in C^2(\overline{\Omega}_j)$ and Δu_j is constant in Ω_j, $\partial^2 u_j/\partial x_i \partial x_k$, $1 \leq i, k \leq n$, must be bounded as $\boldsymbol{x}$ approaches to $\partial\Omega_j$. Therefore, this leads to at least C^2 smoothness of the residual v_j across the block boundary when it is extended by the even reflection. Thus, we can apply Theorem 1 with $m = 2$, and consequently, we have the following.

Corollary 4: Let Ω_j be a bounded rectangular domain in $\mathbb{R}^n$, and let $f_j \in C^2(\overline{\Omega}_j)$, but non-periodic. Assume further that $(\partial/\partial x_i)^3 f$, $i = 1, \ldots, n$, exist and are of bounded variation. Furthermore, let $f_j = u_j + v_j$ be the PHLCT representation, i.e., the polyharmonic component u_j is the solution to (6), and $v_j = f_j - u_j$ is the residual component. Then, the Fourier cosine coefficients of the residual v_j is of $O\left(\|\boldsymbol{k}\|^{-4}\right)$ for all $\boldsymbol{k} \neq \boldsymbol{0}$, where $\boldsymbol{k} = (k_1, \ldots, k_n) \in \mathbb{Z}_+^n$.

IV. Computation of PHLCT from DCT Coefficients

In the previous section, we have derived the asymptotic behavior of PHLCT in the spatial-frequency domain in $\mathbb{R}^n$, $n \in \mathbb{N}$. From now on, we shall only deal with two-dimensional images (i.e., $n = 2$). Furthermore, we shall focus on the analysis of one image block Ω_j for a particular j until we reach Section IV-B. Therefore, for simplicity, we drop the subscript j that was used in many equations appeared in the previous section. Without loss of generality, we also assume $\Omega = (0,1)^2 = \{(x,y) \,|\, 0 < x < 1,\, 0 < y < 1\}$, the unit square in $\mathbb{R}^2$. We shall now derive the DCT coefficients of the u component *directly* from the DCT coefficients of the original data f. Consequently, we shall achieve the PHLCT representation of the original data *in the DCT domain*, which leads us to our new compression-decompression algorithms as we shall examine in detail in Section VI.

Advanced Coding Exhibit No. 2005, IPR2024-00374
Page 008

Let $f(x,y)$ be in $C^2(\overline{\Omega})$. Assume that we are given the discretized version of f sampled at $(x_i,\, y_j) \in \Omega$ for $i,j = 0,1,\ldots,N-1$, where $x_i = (0.5+i)/N$ and $y_j = (0.5+j)/N$. Let $F = (F_{k_1,k_2})$ be a matrix of size $N \times N$, whose entries are the 2D-DCT coefficients of f defined as

$$F_{k_1,k_2} :=$$

$$\lambda_{k_2}\sqrt{\frac{2}{N}}\sum_{j=0}^{N-1}\lambda_{k_1}\sqrt{\frac{2}{N}}\sum_{i=0}^{N-1} f(x_i,\, y_j)\cos\pi k_1 x_i\, \cos\pi k_2 y_j, \tag{7}$$

where $k_1, k_2 = 0,1,\ldots,N-1$ and

$$\lambda_k := \begin{cases} 1/\sqrt{2} & \text{if } \ k=0, \\ 1 & \text{otherwise.} \end{cases} \tag{8}$$

Let us denote the 2D-DCT coefficient matrix of the u component, i.e., the solution of (6), by U. The objective of this section is to compute U when the 2D-DCT coefficient matrix of the original data F is available. Clearly, once U is computed, the 2D-DCT coefficients of the residual are easily available via $V = F - U$.

A. Computing U assuming the ideal boundary condition

We shall now solve Poisson's equation with the Neumann boundary condition (6). Let us assume for the moment that the following discretized Neumann boundary data on the unit square Ω are available:

$$\begin{aligned} &g_i^{(1)} := -f_y(x_i,0), \;\; g_i^{(2)} := f_y(x_i,1), \;\; g_j^{(3)} := -f_x(0,y_j), \\ &g_j^{(4)} := f_x(1,y_j), \quad i,j = 0,1,\ldots,N-1\,, \end{aligned} \tag{9}$$

where $f_x := \partial f(x,y)/\partial x$ and $f_y := \partial f(x,y)/\partial y$, respectively. In practice, the righthand sides of (9) are not readily available, and need to be estimated from the image samples. In Section IV-B, we shall derive a practical method to approximate the righthand sides of (9) using the DCT coefficients of the original data in the current and adjacent blocks, which will be used in our implementation. Let us now consider the following finite Fourier cosine series of the Neumann boundary data:

$$\begin{aligned} g^{(\ell)}(t) &:= \sqrt{\frac{2}{N}}\sum_{k=0}^{N-1}\lambda_k\, G_k^{(\ell)}\cos\pi k t\,, \\ &= \sqrt{\frac{2}{N}}\left(\frac{G_0^{(\ell)}}{\sqrt{2}} + \sum_{k=1}^{N-1} G_k^{(\ell)}\cos\pi k t\right), \\ &\qquad\qquad 0 \le t \le 1\,, \qquad \ell = 1,2,3,4\,, \end{aligned}$$

Advanced Coding Exhibit No. 2005, IPR2024-00374
Page 009

where λ_k was already defined in (8), and $\left\{G_k^{(\ell)}\right\}_{0\le k\le N-1}$ are the 1D-DCT coefficients determined by the boundary data $\left\{g_j^{(\ell)}\right\}_{0\le j\le N-1}$ in (9). Clearly $g^{(\ell)}(t_j)=g_j^{(\ell)}$, where $t_j=(0.5+j)/N$, $j=0,1,\ldots,N-1$, and $\ell=1,\ldots,4$. Now, it is straightforward to show that for $\ell=1$, the function

$$u^{(1)}(x,y):=\sqrt{\frac{2}{N}}\left(\frac{G_0^{(1)}}{\sqrt{2}}\frac{(y-1)^2}{2}\right.$$
$$\left.+\sum_{k=1}^{N-1}G_k^{(1)}\frac{\cosh\pi k(y-1)}{\pi k\sinh\pi k}\cos\pi kx\right)$$

satisfies the following Poisson's equation with the Neumann boundary condition:

$$\begin{cases}\Delta u^{(1)}=\dfrac{1}{|\Omega|}\displaystyle\int_0^1 g^{(1)}(t)\,\mathrm{d}t=\dfrac{G_0^{(1)}}{\sqrt{N}} & \text{in } \Omega,\\[2ex] \dfrac{\partial u^{(1)}}{\partial\nu}=\begin{cases}g^{(1)} & \text{on} \quad \Gamma^{(1)},\\ 0 & \text{on} \quad \partial\Omega\backslash\Gamma^{(1)},\end{cases}\end{cases}$$

where $\Gamma^{(1)}:=\{(x,y)\in\partial\Omega\,|\,0\le x\le 1,\ y=0\}$. See also Figure 1. Similarly, we can derive $u^{(\ell)}$ for $\ell=2,3,4$, and consequently we obtain the solution of (6) as follows:

$$\begin{aligned}u(x,y)&=u^{(1)}(x,y)+u^{(2)}(x,y)+u^{(3)}(x,y)+u^{(4)}(x,y)\\ &=\sqrt{\frac{2}{N}}\sum_{k=0}^{N-1}\lambda_k\left\{\Big(G_k^{(1)}\psi_k(y-1)+G_k^{(2)}\psi_k(y)\Big)\cos\pi kx\right.\\ &\left.+\Big(G_k^{(3)}\psi_k(x-1)+G_k^{(4)}\psi_k(x)\Big)\cos\pi ky\right\}+c\,,\end{aligned}\tag{10}$$

where c is an arbitrary constant that will be determined shortly and

$$\psi_k(t):=\begin{cases}t^2/2 & \text{if } \ k=0,\\ \cosh\pi kt/(\pi k\sinh\pi k) & \text{otherwise.}\end{cases}$$

We note that we derived the solution (10) by modifying the highly accurate Dirichlet problem solver developed by Averbuch, Israeli, and Vozovoi [24] for our Neumann problem. By applying 2D DCT to (10), we finally obtain U_{k_1,k_2}, $k_1,k_2=0,1,\ldots,N-1$, as follows:

$$U_{k_1,k_2}=G_{k_1}^{(1)}\eta_{k_1,k_2}+G_{k_1}^{(2)}\eta^*_{k_1,k_2}+G_{k_2}^{(3)}\eta_{k_2,k_1}+G_{k_2}^{(4)}\eta^*_{k_2,k_1},\tag{11}$$

where

$$\eta_{k,m}:=\lambda_m\sqrt{\frac{2}{N}}\sum_{i=0}^{N-1}\psi_k(x_i-1)\cos\pi mx_i\,,$$

$$\eta^*_{k,m}:=\lambda_m\sqrt{\frac{2}{N}}\sum_{i=0}^{N-1}\psi_k(x_i)\cos\pi mx_i\,.\tag{12}$$

Advanced Coding Exhibit No. 2005, IPR2024-00374
Page 010

TABLE I

NUMERICAL VALUES OF $\eta_{k,m}$ COMPUTED UP TO FOUR DECIMAL PLACES

	$m=0$	$m=1$	$m=2$	$m=3$	$m=4$	$m=5$	$m=6$	$m=7$
$k=0$	0.6641	0.4026	0.0986	0.0421	0.0221	0.0126	0.0070	0.0032
$k=1$	0.4027	0.2000	0.0783	0.0376	0.0206	0.0120	0.0067	0.0031
$k=2$	0.0988	0.0785	0.0480	0.0283	0.0171	0.0104	0.0060	0.0028
$k=3$	0.0425	0.0380	0.0285	0.0197	0.0132	0.0085	0.0051	0.0024
$k=4$	0.0229	0.0214	0.0177	0.0135	0.0097	0.0066	0.0041	0.0020
$k=5$	0.0139	0.0132	0.0115	0.0093	0.0071	0.0051	0.0032	0.0016
$k=6$	0.0090	0.0087	0.0078	0.0066	0.0052	0.0038	0.0025	0.0012
$k=7$	0.0061	0.0060	0.0054	0.0047	0.0038	0.0028	0.0019	0.0009

Note that $\eta_{k,m}$ and $\eta^*_{k,m}$ are independent from any image sample values: once the number of samples N is fixed, they are completely determined and precomputed independently from an input image. For the convenience of the reader, the values of $\eta_{k,m}$ for $N=8$ are listed in Table I. Finally, we determine the constant c in (10) so that $U_{0,0}=0$. In fact, from (11), (12), we can explicitly determine this constant:

$$c = -\frac{4N^2-1}{24N^{2.5}}\left(G_0^{(1)}+G_0^{(2)}+G_0^{(3)}+G_0^{(4)}\right).$$

Thanks to Theorem 1, the decay rate of the DCT coefficients of the residual $V_{\boldsymbol{k}} = F_{\boldsymbol{k}} - U_{\boldsymbol{k}}$ for $\boldsymbol{k} = (k_1,k_2) \neq (0,0)$ should be $O(\|\boldsymbol{k}\|^{-4})$.

B. Approximation of the Neumann boundary condition

In practice, the Neumann boundary data, i.e., the righthand sides of (9), need to be estimated from the image samples. To do so, we need not only the image samples of the current block but also those of the adjacent blocks. Let us consider the four blocks adjacent to Ω as shown in Figure 1. We assume that f is also defined on these adjacent blocks and sampled with the same rate as the current (or center) block Ω. Let us denote the image samples on each block $\Omega^{(s,t)}$ in Fig. 1 by $f_{i,j}^{(s,t)} := f(x_i+s, y_j+t)$, $i,j = 0,1,\ldots,N-1$. For convenience, let us also set $\Omega^{(0,0)} = \Omega$ and $f_{i,j}^{(0,0)} = f(x_i,y_j)$. We now

Advanced Coding Exhibit No. 2005, IPR2024-00374
Page 011

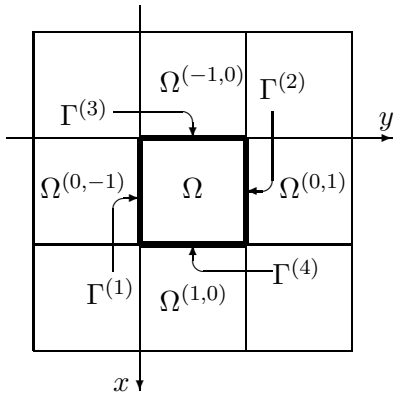

Fig. 1. The configuration of the adjacent blocks and boundary segments of Ω.

approximate the normal derivatives at the boundary of Ω as follows.

$$g_i^{(1)} \simeq X_i^{(-1)} - X_i^{(0)}, \;\; g_i^{(2)} \simeq X_i^{(1)} - X_i^{(0)},$$
$$g_j^{(3)} \simeq Y_j^{(-1)} - Y_j^{(0)}, \;\; g_j^{(4)} \simeq Y_j^{(1)} - Y_j^{(0)}, \tag{13}$$

where

$$X_i^{(t)} := \frac{1}{N}\sum_{j=0}^{N-1} f_{i,j}^{(0,t)}\,,\; Y_j^{(s)} := \frac{1}{N}\sum_{i=0}^{N-1} f_{i,j}^{(s,0)}\,,$$

are the row-wise and column-wise averages, respectively. Let $F^{(s,t)} = \left(F_{k_1,k_2}^{(s,t)}\right)$ be the DCT coefficient matrix of $f^{(s,t)}$ on $\Omega^{(s,t)}$. Then, using (7) and (13), we can express each 1D-DCT coefficient $G_k^{(1)}$ of the Neumann data $g^{(1)}$ as a simple function of *the first column* of the 2D-DCT coefficients of the current and the adjacent blocks as follows:

$$\begin{aligned} G_k^{(1)} &= \lambda_k \sqrt{\frac{2}{N}} \sum_{i=0}^{N-1} g_i^{(1)} \cos \pi k x_i \\ &\simeq \lambda_k \sqrt{\frac{2}{N}} \sum_{i=0}^{N-1} \left\{ X_i^{(-1)} - X_i^{(0)} \right\} \cos \pi k x_i \\ &= \frac{1}{\sqrt{N}} (F_{k,0}^{(0,-1)} - F_{k,0})\,, \qquad k = 0, 1, \ldots, N-1\,, \end{aligned}$$

where λ_k was defined in (8). Similarly we have

$$G_k^{(2)} \simeq \frac{1}{\sqrt{N}}(F_{k,0}^{(0,1)} - F_{k,0}), G_k^{(3)} \simeq \frac{1}{\sqrt{N}}(F_{0,k}^{(-1,0)} - F_{0,k}),$$
$$G_k^{(4)} \simeq \frac{1}{\sqrt{N}}(F_{0,k}^{(1,0)} - F_{0,k}),$$

Advanced Coding Exhibit No. 2005, IPR2024-00374
Page 012

which are simple functions of either the first column or the first row of the 2D-DCT coefficients of the current and adjacent blocks. Inserting these into (11), we have the U_{k_1,k_2} for the approximate discretized Neumann data as

$$\begin{aligned} U_{k_1,k_2} = \frac{1}{\sqrt{N}} \Big\{ & (F^{(0,-1)}_{k_1,0} - F_{k_1,0})\eta_{k_1,k_2} \\ & + (F^{(0,1)}_{k_1,0} - F_{k_1,0})\eta^*_{k_1,k_2} + (F^{(-1,0)}_{0,k_2} - F_{0,k_2})\eta_{k_2,k_1} \\ & + (F^{(1,0)}_{0,k_2} - F_{0,k_2})\eta^*_{k_2,k_1} \Big\} , \end{aligned} \tag{14}$$

for all $k_1,\ k_2 = 0, 1, \ldots, N-1$ except $k_1 = k_2 = 0$. As we mentioned before, $U_{0,0}$, the DC component of u, vanishes. Hence the DC component of the original data f is carried over to that of the v component, i.e., $F_{0,0} = V_{0,0}$. This will become important for our further modification of PHLCT algorithm in Section V and our new compression-decompression algorithms in Section VI.

In the above discussion, we have approximated the first normal derivatives at the block boundary by using the DCT coefficients of the current and its adjacent blocks. Clearly, this approximation scheme is not applicable to the outmost blocks of an input image where some of their adjacent blocks do not exist. In such a case, we set the Neumann boundary function simply by zero, i.e., $g^{(\ell)}(t) = 0$ for appropriate ℓ.

V. Modifying PHLCT for Practice

At this point, let us consider what information must be stored in the forward PHLCT described in the previous section in order to recover the original data f on the block Ω. Both U and V are of course necessary in order to recover f exactly. However, we do not need to store all these $2N^2$ coefficients in PHLCT. Note that each U_{k_1,k_2} is a simple function of the first column or row of the 2D-DCT coefficients of the current and adjacent blocks. Therefore, in order to exactly recover f of the current block, we just need $N^2 + 6N - 2$ coefficients: N^2 for all the entries of V; $6N$ for $F_{k_1,0}$, F_{0,k_2}, $F^{(0,-1)}_{k_1,0}$, $F^{(0,1)}_{k_1,0}$, $F^{(-1,0)}_{0,k_2}$, $F^{(1,0)}_{0,k_2}$ where $k_1, k_2 = 0, 1, \ldots N-1$; and -2 for counting the DC component $F_{0,0}$ three times (note that $F_{0,0} = V_{0,0}$). Considering an application of PHLCT to image compression, this situation is not desirable although it may be acceptable for other purposes such as interpolation, zooming, feature extraction, etc. What we want to have is to recover f exactly from V with the smallest possible number of DCT coefficients from the adjacent blocks. It turns out that we can manage to recover f exactly by $N^2 + 4$ coefficients: N^2 for V and 4 for the DC components of the adjacent blocks. To do so, we need to modify both u and v components in the original PHLCT. In the forward PHLCT, we construct the

Advanced Coding Exhibit No. 2005, IPR2024-00374
Page 013

modified version of U denoted by $\widetilde{U}$ as follows:

$$\widetilde{U}_{k_1,k_2} := \begin{cases} 0 & \text{if } k_1 = k_2 = 0; \\ \frac{1}{\sqrt{N}} \Big\{ (F_{0,0}^{(-1,0)} - F_{0,0})\eta_{0,k_1} & \\ \quad +(F_{0,0}^{(1,0)} - F_{0,0})\eta_{0,k_1}^* \Big\} & \text{if } k_1 \neq 0 = k_2; \\ \frac{1}{\sqrt{N}} \Big\{ (F_{0,0}^{(0,-1)} - F_{0,0})\eta_{0,k_2} & \\ \quad +(F_{0,0}^{(0,1)} - F_{0,0})\eta_{0,k_2}^* \Big\} & \text{if } k_1 = 0 \neq k_2; \\ U_{k_1,k_2} & \text{otherwise,} \end{cases} \tag{15}$$

where U_{k_1,k_2} is defined in (14). In essence, the only difference between U and $\widetilde{U}$ are their first columns and rows, and those of $\widetilde{U}$ can be computed *only using the DC components of the current and adjacent blocks of the originals*. Recall that the first column and row of F are necessary to compute those of U; examine (14) by setting $k_1 = 0$ or $k_2 = 0$. Once we obtain $\widetilde{U}$, then we complete the forward PHLCT by computing the modified residual $\widetilde{V}$ simply by $F - \widetilde{U}$. More explicitly, we compute

$$\widetilde{V}_{k_1,k_2} := \begin{cases} F_{0,0} & \text{if } k_1 = k_2 = 0; \\ F_{k_1,0} - \frac{1}{\sqrt{N}} \Big\{ (F_{0,0}^{(-1,0)} - F_{0,0})\eta_{0,k_1} & \\ \quad +(F_{0,0}^{(1,0)} - F_{0,0})\eta_{0,k_1}^* \Big\} & \text{if } k_1 \neq 0 = k_2; \\ F_{0,k_2} - \frac{1}{\sqrt{N}} \Big\{ (F_{0,0}^{(0,-1)} - F_{0,0})\eta_{0,k_2} & \\ \quad +(F_{0,0}^{(0,1)} - F_{0,0})\eta_{0,k_2}^* \Big\} & \text{if } k_1 = 0 \neq k_2; \\ F_{k_1,k_2} - U_{k_1,k_2} & \text{otherwise.} \end{cases} \tag{16}$$

As for the storage, we only store $\widetilde{V}$ in each block, nothing more. It is important to have $\widetilde{V}_{0,0} = F_{0,0}$.

Let us now consider the inverse PHLCT. Given the 2D-DCT coefficients $\widetilde{V}$, it is clear that we can reconstruct the original data f as follows: 1) Recover the first column and row of F (including the DC component) using $\widetilde{V}$ and the DC components of the adjacent blocks via (16); 2) Compute $\widetilde{U}$ via (15) and the results of Step 1; 3) Set $F = \widetilde{U} + \widetilde{V}$; 4) Apply Inverse 2D DCT to F to recover f.

It is now obvious that the forward and inverse PHLCT algorithms of this modified version, in particular, the inverse algorithm, become much simpler than those of the original PHLCT in the previous section. However, it is natural to ask what we have lost instead. Because of the uniqueness theorem [27, Sec. 2D, 3E] (modulo an additive constant), it is true that, the $\widetilde{u}$ component, the inverse DCT of $\widetilde{U}$,

Advanced Coding Exhibit No. 2005, IPR2024-00374
Page 014

does not satisfy Poisson's equation (6) unlike the u component in the previous section. This means that $\widetilde{u}$ does not satisfy Theorem 3 anymore. However, in terms of the Neumann boundary condition, it is easy to show that $\partial\widetilde{u}/\partial\nu = \partial u/\partial\nu$ on $\partial\Omega$, since the difference

$$\begin{aligned} u - \widetilde{u} = \frac{\sqrt{2}}{N\sqrt{N}} \sum_{k=1}^{N-1} \Big[\{ \, (F_{k,0}^{(0,-1)} - F_{k,0})\eta_{k,0} \\ + (F_{k,0}^{(0,1)} - F_{k,0})\eta_{k,0}^{*} \, \} \cos \pi k x \\ + \{ \, (F_{0,k}^{(-1,0)} - F_{0,k})\eta_{k,0} + (F_{0,k}^{(1,0)} - F_{0,k})\eta_{k,0}^{*} \, \} \cos \pi k y \Big] \end{aligned}$$

clearly satisfies $\partial(u - \widetilde{u})/\partial\nu = 0$ on $\partial\Omega$ thanks to the cosine terms above. Thus, it is still true that $\partial\widetilde{v}/\partial\nu = 0$ on $\partial\Omega$, and consequently $\widetilde{V}_{\boldsymbol{k}} = O(\|\boldsymbol{k}\|^{-4})$. Hence in practice, we have not lost any thing.

From now on, we shall not use the original PHLCT of the previous section, and only use the modified version developed in this section. Therefore, to simplify our notation, we shall drop $\widetilde{}$ and simply use U and V for $\widetilde{U}$ and $\widetilde{V}$.

VI. Application of PHLCT to Image Compression

In this section we propose new compression-decompression algorithms using PHLCT and show its practical advantage over the JPEG Baseline method.

A. Brief review of the lossy JPEG image compression standard

In the JPEG Baseline method, the amount of compression and the quality of reconstructed images is controlled by an 8×8 *quantization table*. Let Q be a quantization table to be used and let $Q_{\boldsymbol{k}} \, (\geq 1)$ be the $\boldsymbol{k}$th entry of Q, where $\mathcal{K} := \{\boldsymbol{k} = (k_1, \, k_2) \mid k_1, k_2 = 0, 1, 2, \ldots, 7 \, \}$. Then DCT coefficients $\{F_{\boldsymbol{k}}\}$ in each block is quantized simply by

$$i_{\boldsymbol{k}} := \text{round}(F_{\boldsymbol{k}}/Q_{\boldsymbol{k}}); \quad F_{\boldsymbol{k}}^{Q} := Q_{\boldsymbol{k}} \times i_{\boldsymbol{k}}, \quad \boldsymbol{k} \in \mathcal{K} \, . \tag{17}$$

This scheme truncates any DCT coefficient $F_{\boldsymbol{k}}$ with $|F_{\boldsymbol{k}}| < Q_{\boldsymbol{k}}/2$. Although the JPEG standard allows one to use any user-supplied quantization table, the most commonly used one is a scalar multiple of the standard Luminance Quantization Table (LQT) shown in Table II. These values were determined by extensive psychophysical experiments on the visibility of the DCT basis vectors [1, Sec. 4.1.3].

The user can change the values of this standard LQT by specifying a parameter called the *quality factor* ranging from 0 (the worst reconstruction quality and the best amount of compression) to 100 (the best reconstruction quality and the worst amount of compression). Let T be an 8×8 matrix whose entries

Advanced Coding Exhibit No. 2005, IPR2024-00374
Page 015

TABLE II

THE LUMINANCE QUANTIZATION TABLE RECOMMENDED BY THE JPEG STANDARD.

	$k_2=0$	$k_2=1$	$k_2=2$	$k_2=3$	$k_2=4$	$k_2=5$	$k_2=6$	$k_2=7$
$k_1=0$	16	11	10	16	24	40	51	61
$k_1=1$	12	12	14	19	26	58	60	55
$k_1=2$	14	13	16	24	40	57	69	56
$k_1=3$	14	17	22	29	51	87	80	62
$k_1=4$	18	22	37	56	68	109	103	77
$k_1=5$	24	35	55	64	81	104	113	92
$k_1=6$	49	64	78	87	103	121	120	101
$k_1=7$	72	92	95	98	112	100	103	99

are the standard LQT shown in Table II. Let q be the qualify factor. Then, the actual quantization table Q for 8 bit grayscale images is typically computed as

$$\begin{aligned} Q_{\boldsymbol{k}} &= Q_{\boldsymbol{k}}(T_{\boldsymbol{k}}; q) \\ &= \begin{cases} \min\left(\text{round}\left(\frac{50 \cdot T_k}{q}\right), 255\right) & \text{if } 0 \le q \le 50; \\ \max\left(\text{round}\left(\frac{(100-q) \cdot T_k}{50}\right), 1\right) & \text{if } 50 \le q \le 100. \end{cases} \end{aligned} \tag{18}$$

Note that when $q = 100$, then $Q_{\boldsymbol{k}} = 1$ for all $\boldsymbol{k}$. In this case the loss due to the quantization is minimum (only the rounding operation is applied directly to the DCT coefficients).

After the quantization, the DC component is encoded as the difference from the DC term of the previous block because the DC components of the adjacent blocks usually correlates strongly and the differential encoding further reduces such correlation or redundancy. The integer sequence $\{i_{\boldsymbol{k}}\}$ in (17) is then ordered into the "zig-zag" sequence, and encoded by some lossless entropy coder, e.g., the Huffman or arithmetic coder, to further compress the sequence before transmitting or storing it.

To decompress the compressed representation, the integer sequence $\{i_{\boldsymbol{k}}\}$ in (17) is first recovered by the decoding algorithm corresponding to the lossless encoder followed by undoing the zig-zag ordering. Then the quantized coefficient matrix F^Q is recovered via (17). Finally, the 2D inverse DCT (IDCT) is applied to F^Q. For the details, see [1], [2].

Advanced Coding Exhibit No. 2005, IPR2024-00374
Page 016

B. *"Full mode" PHLCT: Further reduction of JPEG-DCT bit-rate*

As shown in Section III, PHLCT can improve the decay rate of the DCT coefficients up to $O(\|\boldsymbol{k}\|^{-4})$ compared to $O(\|\boldsymbol{k}\|^{-2})$ if the approximations of the normal derivatives given by (13) are effective. This means that *for the same prescribed quality, the bit-rate should be reduced by PHLCT.* We shall demonstrate our claim by numerical experiments in Section VII.

Let us now propose our new compression/decompression algorithm using our modified PHLCT detailed in Section V. We shall call our new algorithm the "full mode" PHLCT (or simply PHLCT for short) because this is a full and direct application of our decomposition and reconstruction algorithms in Section V to image compression/decompression, which requires modifying both the encoder part and the decoder part of the JPEG Baseline method. We can summarize our proposed algorithm as follows:

Compression:

- • Divide an input image into blocks of 8×8 pixels.
- • Apply DCT to compute F in each block.
- ○ Compute U via (15) and (14) and set $V = F - U$.
- • Quantize V via $i_{\boldsymbol{k}} = \text{round}(V_{\boldsymbol{k}}/Q_{\boldsymbol{k}})$ and encode $\{i_{\boldsymbol{k}}\}$ in the same way as JPEG.

Reconstruction:

- • Decode $\{i_{\boldsymbol{k}}\}$ and reconstruct V^Q via $V^Q_{\boldsymbol{k}} = Q_{\boldsymbol{k}} \times i_{\boldsymbol{k}}$.
- ○ Compute U^Q via (16), (15), and (14) using V^Q, and construct $U^Q + V^Q$.
- • Apply IDCT to $U^Q + V^Q$ in each block.

The steps marked by white dots are added to the original JPEG standard, and the other steps are exactly the same as the JPEG standard. The details of the new step added in the reconstruction procedure are as follows:

Step 1: For $k_1 \cdot k_2 = 0$, compute $U^Q_{\boldsymbol{k}}$ using (15) with $V^Q_{0,0}\,(= F^Q_{0,0})$.

Step 2: Compute $U^Q_{\boldsymbol{k}}$ for $k_1 \cdot k_2 > 0$ using (14).

Step 3: Approximate $F_{\boldsymbol{k}}$ by $U^Q_{\boldsymbol{k}} + V^Q_{\boldsymbol{k}}$ for all $\boldsymbol{k} \in \mathcal{K}$.

Advanced Coding Exhibit No. 2005, IPR2024-00374
Page 017

The increment of the computational cost compared to the original JPEG standard is mainly due to the computation of U in the encoder and U^Q in the decoder. It is clear from (14) and (15) that the computational cost of U or U^Q is approximately $3\,C_1N^2 + 4\,C_2N^2$ for each block of size $N \times N$ pixels, where C_1 and C_2 denote the unit costs for the arithmetic addition and multiplication, respectively. The values of η_{k_1,k_2}, and $\eta^*_{k_1,k_2}$ are common in all blocks and computed in $O(N^2 \log_2 N)$ operations via FFT; see Table I. These quantities should be computed only once in the encoder and in the decoder. In addition, both the encoder and the decoder clearly require C_1N^2 operations per block for computing $F - U$ and $U^Q + V^Q$, respectively.

C. "Partial mode" of PHLCT: Restoration of truncated JPEG-DCT coefficients

It is of practical interest to have a new decompression algorithm that can: 1) reproduce images of improved quality compared to the ones obtained by the JPEG Baseline method while keeping the same bit rate; and 2) accept JPEG files, i.e., image data already compressed by the JPEG standard. In this section, we shall propose an algorithm to do just that. This means that our algorithm cannot touch the encoder and assumes the availability of the quantized DCT coefficients $F^Q_{\boldsymbol{k}}$ in each block instead of $V^Q_{\boldsymbol{k}}$. This new algorithm will be referred to as the *partial mode* PHLCT (or PPHLCT for short) because it only modifies the decorder part of the JPEG Baseline method unlike the full mode PHLCT.

In short, our key idea in PPHLCT is the use of $U^Q_{\boldsymbol{k}}$ to "fill in" the truncated $F^Q_{\boldsymbol{k}}$ by the encoder. Let us now discuss this idea in details. The amount of data compression in the lossy JPEG standard mainly comes from the truncation of the high frequency DCT coefficients. Now, the asymptotic behavior of $F_{\boldsymbol{k}}$ and the residual $V_{\boldsymbol{k}}$ are given by

$$F_{\boldsymbol{k}} = O(\|\boldsymbol{k}\|^{-2})\,,\ V_{\boldsymbol{k}} = O(\|\boldsymbol{k}\|^{-4}) \quad \text{as} \quad \|\boldsymbol{k}\| \to \infty\,.$$

Hence, we have $F_{\boldsymbol{k}} \simeq U_{\boldsymbol{k}}$ as $\|\boldsymbol{k}\| \to \infty$, although we can only reach $\|\boldsymbol{k}\| = 7\sqrt{2} \approx 10$ when each block consists of 8×8 pixels. However, this observation suggests a possibility to approximately restore the truncated higher frequency components using $U_{\boldsymbol{k}}$. It is important to note that $U_{\boldsymbol{k}}$ can be well approximated even after the quantization thanks to (14) and (15) in which $F^{(s,t)}_{\boldsymbol{k}}$ is replaced by $F^{(s,t)Q}_{\boldsymbol{k}}$. This is because those low frequency coefficients used in the righthand side of (14) and (15) are less affected by the quantization process compared to the higher frequency coefficients. Since it is obvious from (12) that

Advanced Coding Exhibit No. 2005, IPR2024-00374
Page 018

$|\eta_{k_1,k_2}| = |\eta^*_{k_1,k_2}|$, we have the following error estimate using (14) and (15):

$$\begin{aligned}|U_{\boldsymbol{k}} - U^Q_{\boldsymbol{k}}| &\leq \frac{1}{\sqrt{N}}(2E_{k_1,0}|\eta_{k_1,k_2}| + 2E_{k_1,0}|\eta^*_{k_1,k_2}| \\ &\quad +2E_{0,k_2}|\eta_{k_2,k_1}| + 2E_{0,k_2}|\eta^*_{k_2,k_1}|) \\ &= \frac{4}{\sqrt{N}}(E_{k_1,0}|\eta_{k_1,k_2}| + E_{0,k_2}|\eta_{k_2,k_1}|)\end{aligned}$$

for all $\boldsymbol{k} = (k_1, k_2)$, where $E_{\boldsymbol{k}}$ denotes an estimation of the quantization error $\max_{s,t\in\{-1,0,1\}} |F^{(s,t)}_{\boldsymbol{k}} - F^{(s,t)\,Q}_{\boldsymbol{k}}|$.

From these considerations, we propose the following scheme for the approximate restoration of the truncated DCT coefficients:

$$\text{Replace } F^Q_{\boldsymbol{k}} \text{ by } F^Q_{\boldsymbol{k}} + d_{\boldsymbol{k}}\,, \quad d_{\boldsymbol{k}} := \begin{cases} U^Q_{\boldsymbol{k}} \text{ if } \boldsymbol{k} \in \mathcal{K}_t, \\ 0 \quad \text{if } \boldsymbol{k} \in \mathcal{K}\backslash\mathcal{K}_t, \end{cases} \tag{19}$$

where $\mathcal{K}_t := \left\{ \boldsymbol{k} \in \mathcal{K} \;\middle|\; F^Q_{\boldsymbol{k}} = 0 \text{ and } |U^Q_{\boldsymbol{k}}| < Q_{\boldsymbol{k}}/2 \right\}$. In words, the truncated DCT coefficients $F^Q_{\boldsymbol{k}}\,(= 0)$ is replaced by $U^Q_{\boldsymbol{k}}\,(\neq 0)$ if $|U^Q_{\boldsymbol{k}}|$ is as small as $|F_{\boldsymbol{k}}|$.

Unfortunately, this method is not effective enough to eliminate the blocking artifacts that become noticeable and annoying particularly in the case of low bit-rate compression. We therefore propose an additional procedure to reduce the blocking artifacts. Let us now consider the reduction of the blocking artifacts on the boundary $\Gamma^{(1)}$ between the current block Ω and the neighboring block $\Omega^{(0,-1)}$ (see also Fig. 1). The reconstructed image $f^Q(x, y)$ obtained from F^Q of (19) still has the following *mean* discontinuity across the boundary $\Gamma^{(1)}$:

$$\begin{aligned}\delta^{(1)} &= \frac{1}{N}\sum_{i=0}^{N-1}\left(f^Q(x_i, 0-) - f^Q(x_i, 0+)\right) \\ &= \frac{\sqrt{2}}{N}\sum_{k=0}^{N-1}\lambda_k(F^{(0,-1)Q}_{0,k}\cos\pi k - F^Q_{0,k})\,,\end{aligned}$$

where $f^Q(x_i, 0-)$ and $f^Q(x_i, 0+)$ denote the left and right limit values at $y = 0$, respectively, and the second equality follows from the definition of the DCT coefficients (7). In order to remove this discontinuity, we add the following quadratic polynomials to $f^Q(x, y)$ on $\Omega^{(0,-1)}$ and Ω, respectively:

$$\begin{aligned}\phi^{(0,-1)}(x, y) &:= (\alpha y - 1)(y + 1)\frac{\delta^{(1)}}{2}\,, \\ \phi(x, y) &:= (\alpha y - 1)(y - 1)\frac{\delta^{(1)}}{2}\,,\end{aligned}$$

where α denotes a constant to be determined. Since $\phi^{(0,-1)}(x_i, 0) = -\delta^{(1)}/2$ and $\phi(x_i, 0) = \delta^{(1)}/2$, the

Advanced Coding Exhibit No. 2005, IPR2024-00374
Page 019

mean discontinuity across $\Gamma^{(1)}$ vanishes as follows:

$$\frac{1}{N}\sum_{i=0}^{N-1}\{(f^Q(x_i,0-)+\phi^{(0,-1)}(x_i,0)) \\ -(f^Q(x_i,0+)+\phi(x_i,0))\}=0\,.$$

These polynomials do not affect the mean discontinuity computation across the boundary segments other than $\Gamma^{(1)}$ because: 1) $\phi^{(0,-1)}(x,-1)=0$ and $\phi(x,1)=0$; and 2) the mean values of $\phi^{(0,-1)}(x,y)$ and $\phi(x,y)$ along the other boundary segments of Ω and $\Omega^{(0,-1)}$ also vanish if we set the constant $\alpha=(6N^2)/(2N^2+1)$, i.e.,

$$\sum_{j=0}^{N-1}\phi^{(0,-1)}(0,y_j)=\sum_{j=0}^{N-1}\phi^{(0,-1)}(1,y_j)=0\,,$$
$$\sum_{j=0}^{N-1}\phi(0,y_j)=\sum_{j=0}^{N-1}\phi(1,y_j)=0\,.$$

Applying this procedure to $\Gamma^{(2)}$, $\Gamma^{(3)}$, and $\Gamma^{(4)}$, we can remove the discontinuities at the block boundary of Ω. In fact, we add the DCT coefficient matrix $P=(P_{k_1,k_2})$ of the following quadratic polynomial to $F^Q(x,y)$ on each block:

$$p(x,y):=(\alpha y-1)(y-1)\frac{\delta^{(1)}}{2}-(\alpha(1-y)-1)y\frac{\delta^{(2)}}{2} \\ +(\alpha x-1)(x-1)\frac{\delta^{(3)}}{2}-(\alpha(1-x)-1)x\frac{\delta^{(4)}}{2}, \tag{20}$$

where

$$\delta^{(2)}=\frac{\sqrt{2}}{N}\sum_{k=0}^{N-1}\lambda_k(F_{0,k}^{(0,1)Q}-F_{0,k}^{Q}\cos\pi k)\,,$$

$$\delta^{(3)}=\frac{\sqrt{2}}{N}\sum_{k=0}^{N-1}\lambda_k(F_{k,0}^{(-1,0)Q}-F_{k,0}^{Q}\cos\pi k)\,,$$

$$\delta^{(4)}=\frac{\sqrt{2}}{N}\sum_{k=0}^{N-1}\lambda_k(F_{k,0}^{(1,0)Q}-F_{k,0}^{Q}\cos\pi k)\,.$$

By the straightforward computation using (7) and (20), we have

$$P_{k_1,k_2}=\begin{cases}0 & \text{if } k_1=k_2=0;\\ \sqrt{N}\left(\gamma_{k_1}\delta^{(3)}-\gamma_{k_1}^*\delta^{(4)}\right) & \text{if } k_1\neq 0=k_2;\\ \sqrt{N}\left(\gamma_{k_2}\delta^{(1)}-\gamma_{k_2}^*\delta^{(2)}\right) & \text{if } k_1=0\neq k_2;\\ 0 & \text{otherwise,}\end{cases} \tag{21}$$

Advanced Coding Exhibit No. 2005, IPR2024-00374
Page 020

where

$$\gamma_k := \lambda_k \sqrt{\frac{2}{N}} \sum_{i=0}^{N-1} \{(\alpha x_i - 1)(x_i - 1)\} \cos \pi k x_i \,,$$

$$\gamma_k^* := \lambda_k \sqrt{\frac{2}{N}} \sum_{i=0}^{N-1} \{(\alpha(1 - x_i) - 1) x_i\} \cos \pi k x_i \,.$$

Based on the above discussions, we propose the following PPHLCT algorithm that provides better approximation to the original DCT coefficient F than the JPEG Baseline method does:

Compression: Same as the JPEG standard.

Reconstruction:

- Decode the compressed sequence and reconstruct F^Q via (17).
  - ○ Compute U^Q via (15), (14).
  - ○ Compute $d_{\boldsymbol{k}}$ as (19).
  - ○ Compute $P_{\boldsymbol{k}}$ via (21).
  - ○ Replace $F^Q_{\boldsymbol{k}}$ by $F^Q_{\boldsymbol{k}} + d_{\boldsymbol{k}} + P_{\boldsymbol{k}}$ if $|d_{\boldsymbol{k}} + P_{\boldsymbol{k}}| \leq Q_{\boldsymbol{k}}/2$.
- Apply IDCT to F^Q in each block.

The computational cost of PPHLCT is slightly larger than that of the PHLCT decoder due to the computation of $d_{\boldsymbol{k}}$ and $P_{\boldsymbol{k}}$. The computation of $d_{\boldsymbol{k}}$ requires $3N^2$ comparisons per block from (19) if we implement the absolute value computation in (19) simply by the comparison operation. The cost for $P_{\boldsymbol{k}}$ is essentially negligible; in fact, it is of $O(N)$ per block instead of $O(N^2)$ since $P_{\boldsymbol{k}}$ has a nonzero value only if $k_1 \cdot k_2 = 0$ and the values of γ_k, γ_k^* are common for all the blocks.

VII. Numerical Experiments

In this section, we describe our numerical experiments and demonstrate the effectiveness of our methods. The grayscale images "Lenna" and "Barbara" shown in Figure 2 (512×512 pixels, 8 bits/pixel) are used in the experiments.

A. How close U and U^Q are to F ?

As we mentioned in Section III, the u component (or its DCT representation U) can be viewed as a predictor of f (or its DCT representation F) using the gradient information across the block boundary.

Advanced Coding Exhibit No. 2005, IPR2024-00374
Page 021

(a) Lenna (b) Barbara

Fig. 2. Original images (512×512 pixels, 8 bits/pixel grayscale).

Clearly, the U component with good prediction capability helps encoding the residual V in PHLCT. It is also of our interest to know how well the U^Q component predicts the original F in the decoding stage particularly in the case of PPHLCT. (Note that in PHLCT we should be satisfied if the U^Q predicts F as well as U does.) From the viewpoint of prediction, there are several algorithms, [1, Sec. 16.1], [14], [15], [17], [18], which predict three to nine low frequency AC components of F. Therefore, in this section, we shall measure the performance of U and U^Q as a predictor of F and compare the results with those obtained by [1, Sec. 16.1] and [14]. We shall not conduct the comparison with the methods proposed by [15], [17], [18] because: 1) the predictors $\widehat{F}_{\boldsymbol{k}}$ for some range of $\boldsymbol{k}$'s proposed by [15] and [17] in the encoding stage require the values of $F_{\boldsymbol{k}}$ themselves and hence the comparison in the encoding stage with our methods does not make sense. 2) The method in [18] needs an optimization by linear programming in order to predict the low frequency AC components of F, in addition to the same problem described in 1).

The goodness of a given predictor $\widehat{F}_{\boldsymbol{k}}$ of $F_{\boldsymbol{k}}$ for a given input image can be measured by the following quantity:

$$R[\widehat{F}_{\boldsymbol{k}}] := 100 \cdot \left(1 - \frac{\langle\, |F_{\boldsymbol{k}} - \widehat{F}_{\boldsymbol{k}}|\,\rangle}{\langle\, |F_{\boldsymbol{k}}|\,\rangle}\right), \quad k_1, k_2 = 0, 1, \ldots, 7\,,$$

where $\langle\, \cdot\,\rangle$ denotes the mean value over all blocks in the input image (the outmost blocks are not included). If $\widehat{F}_{\boldsymbol{k}}$ perfectly predicts $F_{\boldsymbol{k}}$, then $R[\widehat{F}_{\boldsymbol{k}}] = 100$.

Table III shows the prediction performance of various methods for the first 14 DCT coefficients in the zig-zag order after the DC component, i.e., $F_{\boldsymbol{k}}$ for $\boldsymbol{k} = (0,1), (1,0), \ldots, (0,4)$. In the table, we denote the prediction performance at the encoding stage and the decoding stage by $R_{\boldsymbol{k}}$ and $R^Q_{\boldsymbol{k}}$, respectively. In

Advanced Coding Exhibit No. 2005, IPR2024-00374
Page 022

PHLCT, we set $\widehat{F}_{\boldsymbol{k}} = U_{\boldsymbol{k}}$ in the encoding stage while in the decoding stage $\widehat{F}_{\boldsymbol{k}} = U^Q_{\boldsymbol{k}}$. The performance values in Table III were obtained from V^Q's compressed at 0.3 bits/pixel (bpp) for both images.

As for PPHLCT, it is only applicable for the decoding stage. Thus, we put "NA" (Not Applicable) in the encoder performance column in the table. Recall that the predictor $\widehat{F}_{\boldsymbol{k}} = U^Q$ in the decoder stage is computed from the quantized original F^Q instead of V^Q that PHLCT uses. Hence, the performance should be different from that of the predictor in the decoding stage of PHLCT. In this case, F^Q's were obtained by compressing the original F's at 0.3 bpp, which were also used in the other methods described below.

QSFIT in the table denotes an AC prediction method described in [1, Sec. 16.1]. This method is based on the quadratic surface fitting using the DC components of the current and adjacent blocks. Note that the JPEG standard presents the prediction formulas for the lowest five AC components only, i.e., Eq.(16-2a)–Eq.(16-2e) in the encoding stage and Eq.(16-3a)–Eq.(16-3e) in the decoding stage in [1], and hence recommends (as an option) the prediction of these five AC components only. For comparison with our PHLCT and PPHLCT, however, we computed the prediction performance of those 14 AC components by actually fitting the quadratic surface at each block using true DC components in the encoding stage and using the quantized DC components in the decoding stage instead of using the formulas Eq.(16-2a)–Eq.(16-3e).

LAKHANI in the table denotes another AC prediction method proposed in [14] that is also based on the quadratic surface fitting. We computed the prediction performance of the first nine AC components in the zig-zag order using the prediction formulas of Eq.(7)–Eq.(15) in [14]. We note that we could not compute the performance of all the 14 AC components because we could not derive the equation of the quadratic surface from the constraints used in Fig. 3 of [14], and the detailed derivation was not given in that paper.

Table III shows that all the methods perform better in the low frequency AC components, e.g., $\boldsymbol{k} = (0,1),(1,0)$, than the higher frequency AC components, e.g., $\boldsymbol{k} = (3,1),(1,3)$. It also shows that the results of QSFIT in the encoding stage for predicting $F_{\boldsymbol{k}}$ with $\boldsymbol{k} = (k,0),(0,k)$, $k = 1,\ldots,4$, i.e., the first column and row of F, are exactly the same as those of PHLCT. On the other hand, the QSFIT performance in the decoding stage for those $\boldsymbol{k}$'s is exactly the same as that of PPHLCT. This is because: 1) the first column and row of U are generated from a quadratic surface in the spatial domain as one can see from (15) and (12); 2) this quadratic surface is the same as the one used in QSFIT except the constant term; and 3) the normal derivatives of the quadratic surface are approximated using the DC components of the current and adjacent blocks. However, our methods outperform QSFIT for the other AC components.

Advanced Coding Exhibit No. 2005, IPR2024-00374
Page 023

TABLE III

COMPARISON WITH OTHER AC PREDICTION METHODS

	$R_{\boldsymbol{k}}$ / $R^Q_{\boldsymbol{k}}$ for Lenna				$R_{\boldsymbol{k}}$ / $R^Q_{\boldsymbol{k}}$ for Barbara			
$\boldsymbol{k}$	PHLCT	PPHLCT	QSFIT	LAKHANI	PHLCT	PPHLCT	QSFIT	LAKHANI
$(0,1)$	$28/28$	NA/28	$28/28$	$47/43$	$31/30$	$31/30$	$31/30$	$41/34$
$(1,0)$	$33/32$	NA/32	$33/32$	$50/42$	$34/33$	$34/33$	$34/33$	$47/36$
$(2,0)$	$13/12$	NA/12	$13/12$	$21/17$	$12/12$	$12/11$	$12/11$	$19/14$
$(1,1)$	$11/11$	NA/11	$2.2/2.1$	$12/4.0$	$12/12$	$12/12$	$3.4/3.3$	$-23/-37$
$(0,2)$	$13/12$	NA/12	$13/12$	$20/19$	$12/12$	$12/12$	$12/12$	$18/15$
$(0,3)$	$8.6/8.5$	NA/8.5	$8.6/8.5$	$9.3/8.8$	$6.2/6.2$	$6.2/6.1$	$6.2/6.1$	$5.3/4.6$
$(1,2)$	$6.2/6.0$	NA/5.9	$0.6/0.6$	$-6.6/-14$	$3.8/4.2$	$3.8/3.5$	$0.9/0.9$	$-25/-40$
$(2,1)$	$6.9/6.4$	NA/6.6	$-0.1/-0.1$	$-24/-32$	$4.8/4.6$	$4.8/4.5$	$0.7/0.6$	$-36/-51$
$(3,0)$	$8.4/8.4$	NA/8.2	$8.4/8.2$	$8.8/7.4$	$6.5/6.4$	$6.5/6.3$	$6.5/6.3$	$7.2/5.7$
$(4,0)$	$5.7/5.5$	NA/5.4	$5.7/5.4$	NA	$5.9/5.6$	$5.9/5.7$	$5.9/5.7$	NA
$(3,1)$	$2.8/2.7$	NA/2.7	$0.8/0.8$	NA	$1.3/1.4$	$1.3/1.4$	$0.4/0.4$	NA
$(2,2)$	$4.1/3.8$	NA/3.9	$0.1/0.1$	NA	$1.2/1.4$	$1.2/1.3$	$0.2/0.1$	NA
$(1,3)$	$1.9/1.9$	NA/1.9	$0.5/0.5$	NA	$0.3/0.4$	$0.3/0.4$	$0.1/0.1$	NA
$(0,4)$	$5.7/5.7$	NA/5.6	$5.7/5.6$	NA	$2.5/2.4$	$2.5/2.5$	$2.5/2.5$	NA

Note that the performance of PHLCT in the decoding stage for some $\boldsymbol{k}$'s is slightly different from that of QSFIT and PPHLCT due to the difference in computing the predictor from V^Q and from F^Q. For the first column and row of F, LAKHANI gives the best results. However, the difference between the performance values before and after quantization is larger than the other methods. For example, even at $\boldsymbol{k} = (1,0)$, the performance drop after quantization is more than 10% relative to the true mean value $\langle F_{1,0} \rangle$. Concerning the other range of $\boldsymbol{k}$'s, in particular, at $\boldsymbol{k} = (1,1), (1,2), (2,1)$, our methods and QSFIT perform better than LAKHANI.

B. Image Compression

We now describe our image compression experiments. In addition to the standard LQT with the rule (18), we also introduce a modified version of the rule here. This is based on the following observation

Advanced Coding Exhibit No. 2005, IPR2024-00374
Page 024

from our experiments and experience: the smaller the quantization error of the DC components (regardless of JPEG-DCT, PHLCT, or PPHLCT), the more numerically accurate and the perceptually better the reconstructed images are. In other words, controlling the quantization errors of the DC components is much more important than those of the other higher frequency AC components. Thus, we impose an upper bound on the quantization step size of the DC components in order to keep the accuracy even in the very low bit-rate case. More precisely, the element $Q_{\mathbf{0}}$ in (18) is *modified* as the following rule: *if* $Q_{\mathbf{0}} > M$*, then replace* $Q_{\mathbf{0}}$ *by* M. In other words, the quantization step size for the DC components is always bounded by a constant M, whatever the quality factor q is used. In the experiments below, we set the constant M by an ad hoc procedure, e.g., $M = 0.05 \langle F_{\mathbf{0}} \rangle$, where $\langle F_{\mathbf{0}} \rangle$ denotes the mean value of the DC components of all the blocks of size 8×8 pixels in an input image. We shall denote this modified quantization rule by QM whereas the standard rule (18) by QS.

To measure the performance of compression and decompression objectively, we use the Peak Signal-to-Noise Ratio (PSNR) and the Mean Structural SIMilarity index (MSSIM). PSNR is normally considered a better metric for image quality assessment than SNR and defined as

$$20 \log_{10} \left(\max_{(x,y)\in\Omega} |f^Q(x,y)| / RMSE \right),$$

where Ω is the entire image domain (not a single block of 8×8 pixels) and $RMSE$ (the root mean square error) is the absolute ℓ^2 error between the original image and the reconstruction divided by the square root of the total number of pixels. The unit of PSNR is decibel (dB). MSSIM is a more perceptually-correct measure of similarity between two images that was recently proposed by Wang et al. [28]. This is based on the comparison of the local patterns of pixel intensities normalized for luminance and contrast. If the original image is regarded as the one with the perfect quality, then the MSSIM between the original and the reconstruction can be considered as a quality measure of the reconstructed image. Note that the value of MSSIM becomes 1 if the reconstruction perfectly recovers the original.

Figures 3 and 4 show the comparison between PHLCT, PPHLCT, and the JPEG Baseline method for the images Lenna and Barbara, respectively. In these figures, the quality factor q in (18) was sampled uniformly with the sampling rate $\Delta q = 3$ so that the bit rates take values approximately from 0.15 bpp up to 1.0 bpp, and then the images were compressed accordingly using the rules QM and QS in all cases. The bit rates were computed from the Huffman codes of the quantized data in the zig-zag order. Finally, PSNR and MSSIM were computed after decompressing them. We note that in order to obtain the results indicated by QM, not only the decoder but also the encoder must use the QM rule. Therefore, PPHLCT with QM is effective only when the QM rule has been used in the encoder of the JPEG Baseline method.

Advanced Coding Exhibit No. 2005, IPR2024-00374
Page 025

In Figures 3 and 4, PHLCT(QM) is the overall winner, which was clearly expected, and the improvement over JPEG-DCT by PHLCT and PPHLCT is more clearly shown in MSSIM than in PSNR. In all cases, the performance difference between QS and QM is particularly noticeable for the low bit-rate range smaller than 0.3 bpp. On the other hand, if one can afford to use more than 0.3 bpp, there seems no need to use QM. The improvement by PPHLCT(QS) is the smallest, which was also expected since this is the only case that does not modify the encoder of the JPEG Baseline method at all. The improvement by PPHLCT(QM) is slightly larger than that by PPHLCT(QS) while it is still smaller than that by PHLCT(QS). Even so, there is a practical advantage of PPHLCT(QM) over PHLCT in terms of the compatibility with the JPEG standard encoder: the only difference between the encoder of PPHLCT(QM) and that of the JPEG standard is the standard quantization table whereas more substantial modification is required for the encoder of PHLCT as described in details in Section VI-B. In addition, these figures also indicate that it is tougher to compress the Barbara image than the Lenna image.

In order to show the performance difference more clearly in PSNR, we computed the reduction in the bit rate by PHLCT(QS) and PPHLCT(QS) relative to that of JPEG-DCT(QS) for a given value of PSNR. Similarly we computed the reduction rates for the QM versions. Figure 5 shows our results, which more clearly confirm our observations mentioned above in terms of PSNR.

To show the effect of the compression-decompression quality of each method clearly, we display the face region of the reconstructed Lenna and Barbara images in Figures $6-9$. Note that the bit rates and the PSNR values listed with the images are computed from the entire image, not from the face part. The quality factors that achieved those bit rates and PSNR values are also listed with the images. It is clear that both PHLCT and PPHLCT improved the quality of the JPEG-compressed images under the constraint of keeping the same bit rates. The difference is particularly noticeable for the low bit-rate case (0.15 bpp).

C. Quantification of Blocking Artifacts Reduction

We also evaluated the performance of the reduction of blocking artifacts in the decompressed images by using a measure called the *mean squared difference of slope* (MSDS) proposed in [13] and used (with modification) in [16] and [17]. The MSDS values are computed from the sequences of four consecutive pixel values in horizontal/vertical directions across a block boundary or of four pixel values in diagonal direction at an intersection of diagonally adjacent blocks as in [17]. We computed MSDS for all block boundaries and all intersections in each image. Table IV shows our computational results of MSDS for the Lenna and Barbara images. In this table, MSDSb and MSDSi denote the mean values of MSDS

Advanced Coding Exhibit No. 2005, IPR2024-00374
Page 026

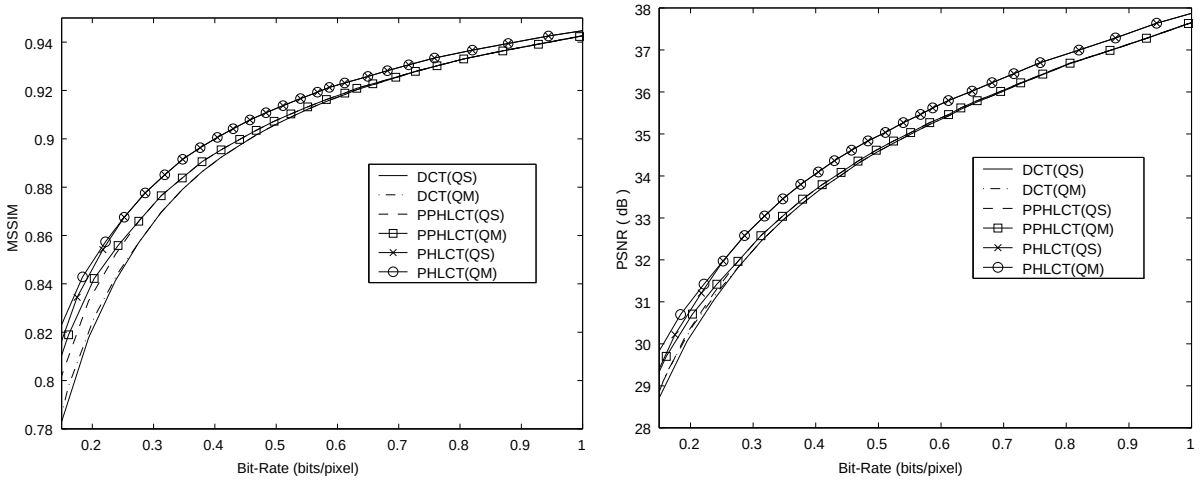

(a) (b)

Fig. 3. Comparison of the compression performance between PHLCT, PPHLCT, and DCT (JPEG Baseline method) for the Lenna image.

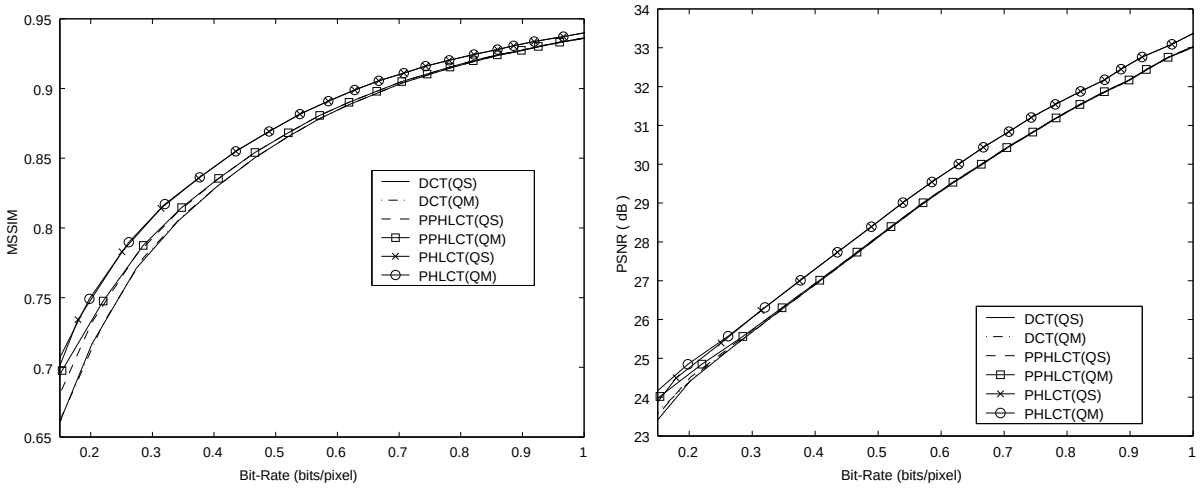

(a) (b)

Fig. 4. Comparison of the compression performance between PHLCT, PPHLCT, and DCT (JPEG Baseline method) for the Barbara image.

Advanced Coding Exhibit No. 2005, IPR2024-00374
Page 027

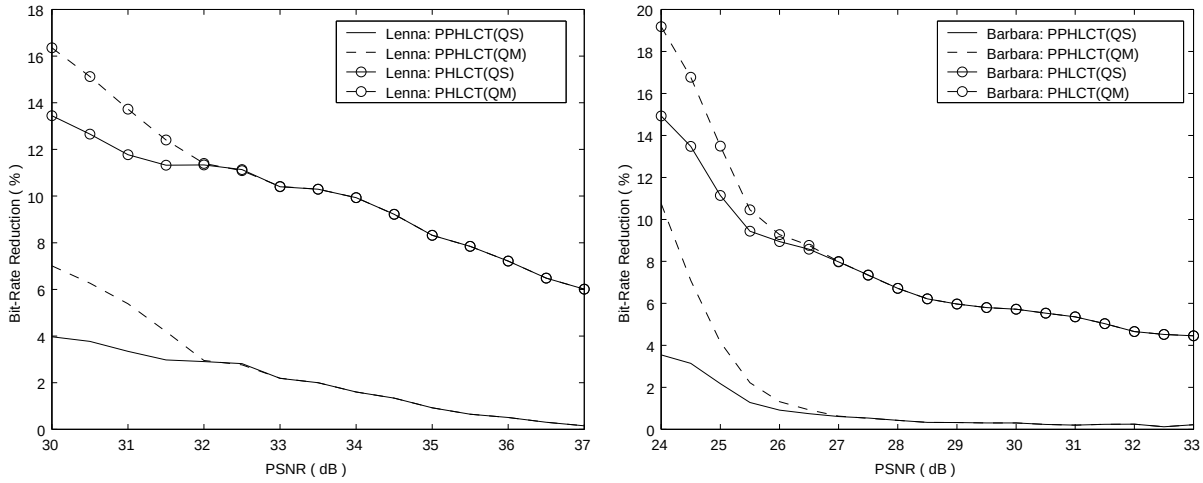

(a) Lenna (b) Barbara

Fig. 5. Bit-rate reduction by PHLCT and PPHLCT over DCT (the JPEG Baseline method) to achieve the same PSNR values.

computed at all the block boundaries and all the intersections, respectively. In all cases of PHLCT and PPHLCT, the values of MSDS decrease compared to the JPEG-DCT cases. There are, however, a couple of interesting things to notice. First, there is no difference between the performance of QS and that of QM for the Lenna images reconstructed from the compressed representations of 0.3 bpp while those of 0.15 bpp show significant difference. This indicates, not surprisingly, that the QM rule may not be not helpful for the higher bit rate compression for relatively smooth images such as the Lenna image. Second, the MSDS values for the Barbara images reconstructed from the compressed representations of 0.3 bpp are larger than those of 0.15 bpp. This is because the intrinsic discontinuities and textures in the original Barbara image had been too much smoothed in the case of 0.15 bpp. However, for each bit rate, the MSDS values of our methods are still smaller than those of the JPEG-DCT. Therefore, we can conclude that both PHLCT and PPHLCT are effective for the reduction of blocking artifacts in terms of MSDS.

VIII. Conclusion

In this paper, we have described two new image compression-decompression schemes that reproduce images with better visual fidelity, less blocking artifacts, and better PSNR, particularly in low bit rates, than those processed by the JPEG Baseline method at the same bit rates. The first one, the "full mode" polyharmonic local cosine transform (or PHLCT for short), modifies both the encoder and decoder parts

Advanced Coding Exhibit No. 2005, IPR2024-00374
Page 028

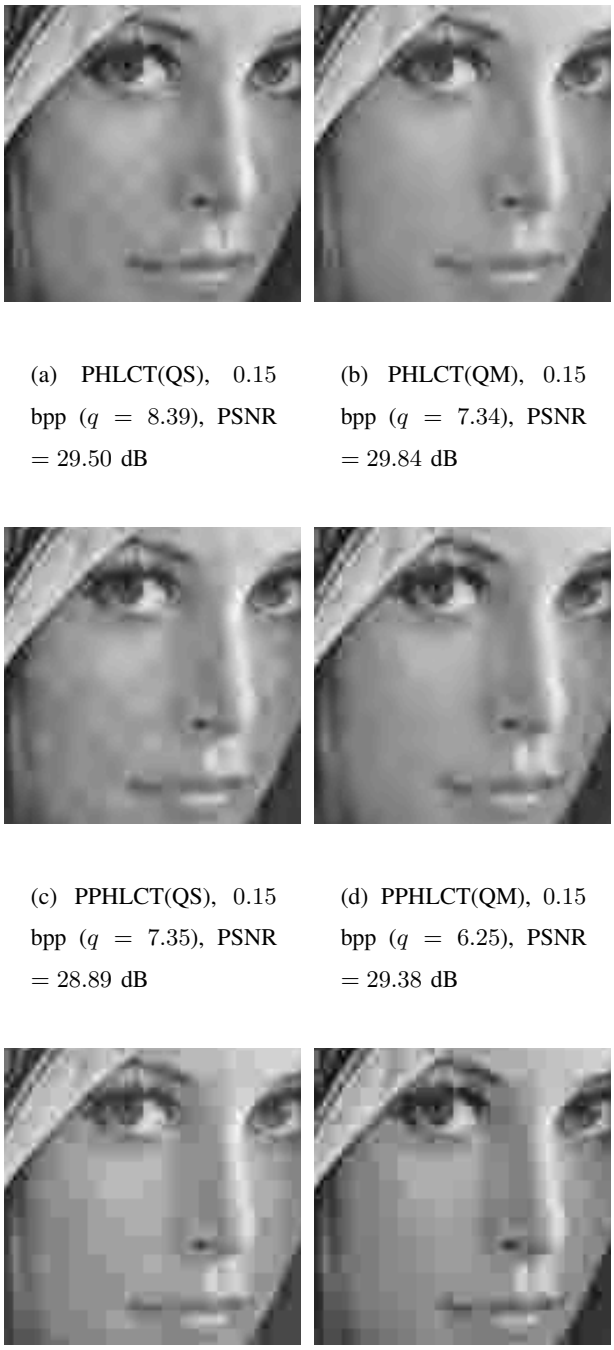

(a) PHLCT(QS), 0.15 bpp ($q = 8.39$), PSNR $= 29.50$ dB

(b) PHLCT(QM), 0.15 bpp ($q = 7.34$), PSNR $= 29.84$ dB

(c) PPHLCT(QS), 0.15 bpp ($q = 7.35$), PSNR $= 28.89$ dB

(d) PPHLCT(QM), 0.15 bpp ($q = 6.25$), PSNR $= 29.38$ dB

(e) DCT(QS), 0.15 bpp ($q = 7.35$), PSNR $= 28.70$ dB

(f) DCT(QM), 0.15 bpp ($q = 6.25$), PSNR $= 28.93$ dB

Fig. 6. The reconstructed Lenna images by PHLCT, PPHLCT, and DCT (the JPEG Baseline method) with 0.15 bpp.

Advanced Coding Exhibit No. 2005, IPR2024-00374
Page 029

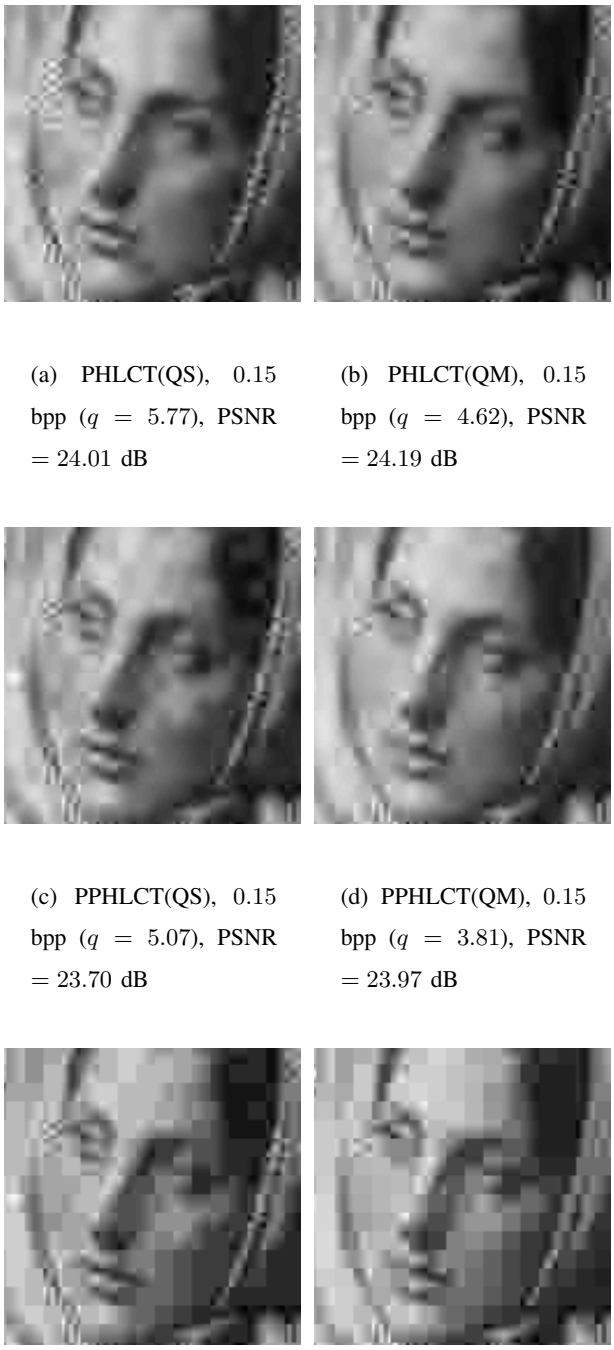

(a) PHLCT(QS), 0.15 bpp ($q = 5.77$), PSNR $= 24.01$ dB

(b) PHLCT(QM), 0.15 bpp ($q = 4.62$), PSNR $= 24.19$ dB

(c) PPHLCT(QS), 0.15 bpp ($q = 5.07$), PSNR $= 23.70$ dB

(d) PPHLCT(QM), 0.15 bpp ($q = 3.81$), PSNR $= 23.97$ dB

(e) DCT(QS), 0.15 bpp ($q = 5.07$), PSNR $= 23.58$ dB

(f) DCT(QM), 0.15 bpp ($q = 3.81$), PSNR $= 23.61$ dB

Fig. 7. The reconstructed Barbara images by PHLCT, PPHLCT, and DCT (the JPEG Baseline method) with 0.15 bpp.

Advanced Coding Exhibit No. 2005, IPR2024-00374
Page 030

(a) PHLCT(QS), 0.3 bpp ($q = 20.3$), PSNR = 32.80 dB

(b) PHLCT(QM), 0.3 bpp ($q = 20.3$), PSNR = 32.80 dB

(c) PPHLCT(QS), 0.3 bpp ($q = 17.95$), PSNR = 32.36 dB

(d) PPHLCT(QM), 0.3 bpp ($q = 17.95$), PSNR = 32.36 dB

(e) DCT(QS), 0.3 bpp ($q = 17.95$), PSNR = 32.22 dB

(f) DCT(QM), 0.3 bpp ($q = 17.95$), PSNR = 32.22 dB

Fig. 8. The reconstructed Lenna images by PHLCT, PPHLCT, and DCT (the JPEG Baseline method) with 0.3 bpp.

Advanced Coding Exhibit No. 2005, IPR2024-00374
Page 031

(a) PHLCT(QS), 0.3 bpp ($q = 12.35$), PSNR = 26.06 dB

(b) PHLCT(QM), 0.3 bpp ($q = 11.97$), PSNR = 26.05 dB

(c) PPHLCT(QS), 0.3 bpp ($q = 11.1$), PSNR = 25.70 dB

(d) PPHLCT(QM), 0.3 bpp ($q = 10.7$), PSNR = 25.73 dB

(e) DCT(QS), 0.3 bpp ($q = 11.1$), PSNR = 25.66 dB

(f) DCT(QM), 0.3 bpp ($q = 10.7$), PSNR = 25.67 dB

Fig. 9. The reconstructed Barbara images by PHLCT, PPHLCT, and DCT (the JPEG Baseline method) with 0.3 bpp.

Advanced Coding Exhibit No. 2005, IPR2024-00374
Page 032

TABLE IV

MSDS OF RECONSTRUCTED IMAGES

	Lenna			Barbara		
	MSDSb	MSDSi	PSNR(dB)	MSDSb	MSDSi	PSNR(dB)
Original	645	379		5190	3082	
DCT(QS), 0.15 bpp	2592	1351	28.70	8876	3833	23.58
DCT(QM), 0.15 bpp	2658	1455	28.93	8360	3593	23.61
PPHLCT(QS), 0.15 bpp	1439	873	28.89	6567	3051	23.70
PPHLCT(QM), 0.15 bpp	1452	932	29.38	5743	2657	23.97
PHLCT(QS), 0.15 bpp	1384	894	29.50	7060	3374	24.01
PHLCT(QM), 0.15 bpp	1372	889	29.84	6120	2893	24.19
DCT(QS), 0.3 bpp	1472	863	32.22	10346	4582	25.66
DCT(QM), 0.3 bpp	1472	863	32.22	10203	4522	25.67
PPHLCT(QS), 0.3 bpp	1080	689	32.36	9177	4222	25.70
PPHLCT(QM), 0.3 bpp	1080	689	32.36	9052	4154	25.73
PHLCT(QS), 0.3 bpp	1062	670	32.80	9116	4167	26.06
PHLCT(QM), 0.3 bpp	1062	670	32.80	9113	4121	26.05

of the JPEG Baseline method. The second one, the "partial mode" PHLCT (or PPHLCT for short), only modifies the decoder part: it accepts the JPEG files, yet decompresses them with higher quality than the JPEG standard. The key idea behind these algorithms is a decomposition of each image block into a *polyharmonic* component and a *residual*. The polyharmonic component in this paper is an approximate solution to Poisson's equation with the Neumann boundary condition, which can be considered as a smooth predictor of the original image block using the image gradient information across the block boundary. The residual—obtained by removing the polyharmonic component from the original image block—has thus approximately zero gradient across the block boundary, which gives rise to the DCT coefficients decaying as $O(\|\boldsymbol{k}\|^{-4})$ whereas those of the original image block decay only as $O(\|\boldsymbol{k}\|^{-2})$. This fast decay rate in turn has led us to more efficient compression-decompression algorithms for the same bit rates. Moreover, we have shown that the polyharmonic component of each block can be estimated solely by the first column and row of the DCT coefficient matrix of that block and those of its adjacent

Advanced Coding Exhibit No. 2005, IPR2024-00374
Page 033

blocks. This is important in two aspects: 1) it provides a simpler decompression algorithm; and 2) it allows us to develop PPHLCT that fills in the truncated small DCT coefficients of the original image due to quantization with the corresponding polyharmonic components.

The additional computational cost incurred by our new methods is small. In addition to the cost of the JPEG Baseline method, both the encoder and decoder parts of PHLCT requires $O(N^2)$ operations per block of size $N \times N$ pixels and $O(N^2 \log_2 N)$ operations to compute Table I or Eq. (12) per image, where typically $N = 8$. The cost of computing Table I is essentially negligible since this is done only once in the encoder as well as in the decoder. As for PPHLCT, it has only a decoder part and requires $O(3N^2)$ comparison operations per block in addition to the cost of the decoder part of PHLCT. Hence we can claim that the additional cost incurred by our methods beyond the JPEG Baseline method is just linearly proportional to the number of pixels in the image.

Our numerical experiments in Section VII have demonstrated that PHLCT and PPHLCT improve the decompressed image quality over the JPEG Baseline method under the constraint of keeping the same bit rates. Here we have used PSNR and MSSIM as a measure of image quality and MSDS to specifically quantify the reduction of blocking artifacts. The subjective image quality is also improved by our methods as shown in Figures 6−9. We have also numerically demonstrated that the polyharmonic component of our methods can predict an original image data better and more stably than the other AC prediction methods such as [1, Sec. 16.1] and [14].

Our future work will include a more thorough investigation of polyharmonic components that may be obtained by a polyharmonic equation of higher degree of polyharmonicity or by a different type of elliptic equation. Furthermore, we are currently generalizing the polyharmonic local trigonometric transform for analyzing objects of various shapes in an image, which we hope to report at a later date.

APPENDIX

PROOF OF THEOREM 3

Proof: Recall that u_j is the solution to the Neumann boundary problem of Poisson's equation (6) (modulo an additive constant).

$$\begin{aligned} M(p) - M(u_j) &= \int_\Omega \left((\Delta p)^2 - (\Delta u_j)^2 \right) \mathrm{d}\boldsymbol{x} \\ &= \int_\Omega (\Delta p - \Delta u_j)^2 \, \mathrm{d}\boldsymbol{x} + 2 \int_\Omega (\Delta p - \Delta u_j) \Delta u_j \, \mathrm{d}\boldsymbol{x} \\ &= \int_\Omega (\Delta p - \Delta u_j)^2 \, \mathrm{d}\boldsymbol{x} + 2K_j \int_\Omega (\Delta p - \Delta u_j) \, \mathrm{d}\boldsymbol{x} \,. \end{aligned}$$

Advanced Coding Exhibit No. 2005, IPR2024-00374
Page 034

Using Green's second identity, we have

$$\int_\Omega (\Delta p - \Delta u_j)\,\mathrm{d}\boldsymbol{x} = \int_{\partial\Omega} \frac{\partial p}{\partial \nu}\,\mathrm{d}\sigma(\boldsymbol{x}) - \int_{\partial\Omega} \frac{\partial u_j}{\partial \nu}\,\mathrm{d}\sigma(\boldsymbol{x}) = 0\,.$$

Therefore

$$M(p) - M(u_j) = \int_\Omega (\Delta p - \Delta u_j)^2\,\mathrm{d}\boldsymbol{x} \geq 0\,.$$

■

ACKNOWLEDGMENT

This research was partially supported by by the ONR grant N00014-00-1-0469 and the NSF grant DMS-0410406. The first author would like to thank Shizuoka University for granting him an opportunity to spend for one year at University of California, Davis, which resulted in this paper. We also would like to thank the anonymous reviewers for their comments and criticisms that have improved this article considerably.

REFERENCES

[1] W. B. Pennebaker and J. L. Mitchell, *JPEG Still Image Data Compression Standard*. New York: Van Nostrand Reinhold, 1993.

[2] G. K. Wallace, "The JPEG still picture compression standard," *IEEE Trans. Consumer Electronics*, vol. 38, no. 1, pp. xviii–xxxiv, 1992.

[3] N. Ahmed, T. Natarayan, and K. R. Rao, "Discrete cosine transform," *IEEE Trans. Comput.*, vol. COM-23, pp. 90–93, 1974.

[4] K. R. Rao and P. Yip, *Discrete Cosine Transform: Algorithms, Advantages, and Applications*. San Diego, CA: Academic Press, 1990.

[5] G. Strang, "The discrete cosine transform," *SIAM Review*, vol. 41, no. 1, pp. 135–147, 1999.

[6] R. J. Clarke, "Relation between the Karhunen Loève and cosine transforms," *IEE Proceedings, Part F*, vol. 128, no. 6, pp. 359–360, Nov. 1981.

[7] D. L. Donoho, M. Vetterli, R. A. DeVore, and I. Daubechies, "Data compression and harmonic analysis," *IEEE Trans. Inform. Theory*, vol. 44, no. 6, pp. 2435–2476, 1998, invited paper.

[8] S. W. Hong, Y. H. Chan, and W. C. Siu, "A new approach for real time reduction of blocking effect," *Signal Processing*, vol. 65, no. 3, pp. 337–346, 1998.

[9] J. Luo, C. W. Chen, K. J. Parker, and T. S. Huang, "Artifact reduction in low bit rate DCT-based image compression," *IEEE Trans. Image Process.*, vol. 5, no. 9, pp. 1363–1368, 1996.

[10] Q. Lu, J. Luo, and R. L. Joshi, "Image processing method for reducing noise and blocking artifact in a digital image," US Patent, No. 6,636,645, Oct. 21, 2003.

[11] Y. Kawasaka, "Block distortion corrector and image signal expander," US Patent, No. 5,949,917, Sep. 7, 1999.

[12] D. Zhang and Z. Wang, "Image information restoration based on long-range correlation," *IEEE Trans. Circ. Syst. Vid.*, vol. 12, no. 5, pp. 331–341, 2002.

Advanced Coding Exhibit No. 2005, IPR2024-00374
Page 035

[13] S. Minami and A. Zakhor, "An optimization approach for removing blocking effects in transform coding," *IEEE Trans. Circ. Syst. Vid.*, vol. 5, no. 2, pp. 74–82, Apr. 1995.

[14] G. Lakhani, "Improved image reproduction from dc components," *Opt. Eng.*, vol. 35, no. 12, pp. 3449–3452, 1996.

[15] ——, "Improved equations for JPEG's blocking artifacts reduction approach," *IEEE Trans. Circ. Syst. Vid.*, vol. 7, no. 6, pp. 930–934, 1997.

[16] G. Lakhani and N. Zhong, "Derivation of prediction equations for blocking effect reduction," *IEEE Trans. Circ. Syst. Vid.*, vol. 9, no. 3, pp. 415–418, Apr. 1999.

[17] G. A. Triantafyllidis, D. Tzovaras, and M. G. Strintzis, "Blocking artifact detection and reduction in compressed data," *IEEE Trans. Circ. Syst. Vid.*, vol. 12, no. 10, pp. 877–890, 2002.

[18] V. T. Kieu and D. T. Nguyen, "Surface fitting approach for reducing blocking artifacts in low bitrate DCT decoded images," in *Proc. 2001 International Conf. Image Proc.* IEEE, 2001, pp. 150–153.

[19] N. Saito and J.-F. Remy, "A new local sine transform without overlaps: A combination of computational harmonic analysis and PDE," in *Wavelets: Applications in Signal and Image Processing X*, M. A. Unser, A. Aldroubi, and A. F. Laine, Eds., vol. Proc. SPIE 5207, 2003, pp. 495–506.

[20] ——, "The polyharmonic local sine transform: A new tool for local image analysis and synthesis without edge effect," *Applied and Computational Harmonic Analysis*, 2005, to appear.

[21] R. R. Coifman and Y. Meyer, "Remarques sur l'analyse de Fourier à fenêtre," *Comptes Rendus Acad. Sci. Paris, Série I*, vol. 312, pp. 259–261, 1991.

[22] H. S. Malvar, "The LOT: transform coding without blocking effects," *IEEE Trans. Acoust., Speech, Signal Process.*, vol. 37, pp. 553–559, 1989.

[23] ——, "Lapped transforms for efficient transform/subband coding," *IEEE Trans. Acoust., Speech, Signal Process.*, vol. 38, pp. 969–978, 1990.

[24] A. Averbuch, M. Israeli, and L. Vozovoi, "A fast Poisson solver of arbitrary order accuracy in rectangular regions," *SIAM J. Sci. Comput.*, vol. 19, no. 3, pp. 933–952, 1998.

[25] E. Braverman, M. Israeli, A. Averbuch, and L. Vozovoi, "A fast 3D Poisson solver of arbitrary order accuracy," *J. Comput. Phys.*, vol. 144, pp. 109–136, 1998.

[26] J. Zhao, N. Saito, and K. Yamatani, "PHLFT5: A practical and improved version of polyharmonic local Fourier transform," in *Wavelets: Applications in Signal and Image Processing XI*, M. Papadakis, , A. F. Laine, and M. A. Unser, Eds., vol. Proc. SPIE 5914, 2005, to appear.

[27] G. B. Folland, *Introduction to Partial Differential Equations*, 2nd ed. Princeton Univ. Press, 1995.

[28] Z. Wang, A. C. Bovik, H. R. Sheikh, and E. P. Simoncelli, "Image quality assessment: From error measurement to structural similarity," *IEEE Trans. Image Process.*, vol. 13, no. 4, pp. 600–613, 2004.

Advanced Coding Exhibit No. 2005, IPR2024-00374
Page 036